



TÜBİTAK

A novel single-inductor eight-channel light-emitting diode driver for low power display backlight applications

Magesh Kannan PARTHASARATHY*, Nagarajan GANESAN

Department of Electronics and Communication Engineering, Pondicherry Engineering College, Puducherry, India

Received: 20.12.2016

Accepted/Published Online: 06.04.2018

Final Version: 27.07.2018

Abstract: A novel decoder-based single-inductor eight-channel light-emitting diode (LED) driver circuit for low power display backlight applications has been proposed. Uniform brightness in the display provides better picture clarity, which can be achieved by providing uniform DC currents to all channels in the backlight arrangement. Existing systems use individual current regulators for each channel, which fails to provide uniform current to individual channels. Instead, uniform current is provided to all eight channels in the proposed system as the same current is distributed to all channels using time-multiplexing by a 3×8 decoder and a 3-bit binary up-counter. A digital pulse width modulator is used in the existing system, which has unwanted switching activities and electromagnetic interference (EMI). Unwanted switching activities and EMI are completely eliminated in the proposed system by applying a novel switching technique. The proposed LED driver is designed and implemented using the 180-nm CMOS process. Each channel is designed to conduct 300 mA of current through it when the supply is 12 V. The proposed LED driver consumes total power of 8.746 W at 27 °C while the peak power efficiency is 96.26%. The minimum current balancing error of the proposed LED driver is 0.019%, whereas it is 0.12% for the existing system. The existing method exhibits an average current balancing error of 2.04% whereas the proposed technique exhibits 1.33% as the average current balancing error, which is 34.82% less than the existing system.

Key words: Backlight, current balancing error, light-emitting diode driver, single-inductor multiple-output

1. Introduction

In recent years, light-emitting diode (LED) displays have gained more popularity because of their vital role in high-definition (HD) televisions, laptops, and smart phones. Due to their higher lumen per watt, better lifespan, fast response time, wider color capacity, and better suitable for green energy, LEDs are being used in display backlighting applications instead of compact fluorescent lights [1–4]. When the display size is larger, multiple-channel LED drivers are used to supply uniform currents to all channels to achieve the best picture clarity. The brightness of the LED string depends on the current flows through them; hence, it is mandatory to supply uniform current through all channels in the display backlight arrangement. Multichannel LED drivers are used to achieve uniform current in all channels [5–7]. A single-inductor eight-channel DC-DC boost converter is designed to supply a total current of 300 mA in the proposed system, which is circulated to all channels based on the time-division multiplexing access method. This provides uniform distribution of current to all eight channels so that uniform brightness is achieved in the proposed system. The conventional individual current regulator-based LED driver is depicted in Figure 1. The channel current in each channel is controlled by the

*Correspondence: maheshkannan@gmail.com

dedicated individual current regulator of each channel in the conventional LED driver. The individual current regulator in each channel fails to supply uniform current in all channels because of temperature and process variations. This causes more current balancing error and the current distribution in the existing conventional LED driver with individual current regulator is not uniform. Hence, the clarity of the picture is affected by the existing LED drivers. In the conventional individual current regulator-based LED driver, the turn-on voltage of the LED is more sensitive to the process. The resistors connected in each channel are more sensitive to temperature. Hence, the current in each channel is not uniform and moreover the variations cause more voltage fluctuations in the existing LED driver, which in turn consumes more power. Hence, the power efficiency is degraded in conventional LED drivers.

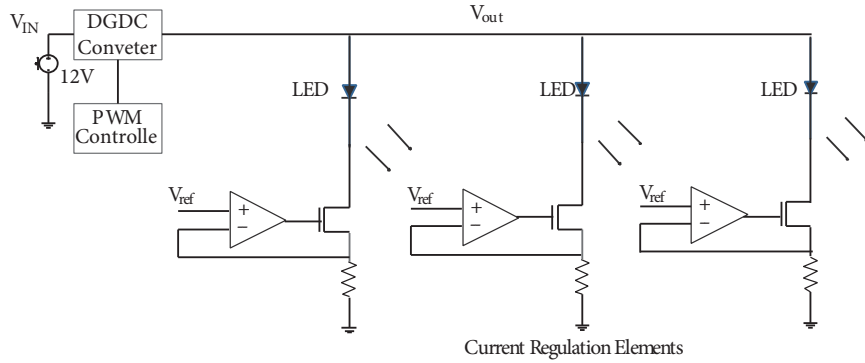


Figure 1. Conventional LED driver with individual current regulator [3].

Uniform current distribution is mandatory to achieve uniform brightness and better clarity of picture in the latest display panels for HD televisions, laptops, and smart phones. Hence, the single-inductor multiple-output (SIMO) DC-DC boost converter plays a vital role in the latest large display backlight applications to provide better picture clarity with uniform brightness. Since the SIMO boost converter topology distributes the uniform current to all channels based on the time-division multiplexing method, the total current balancing error is very small and the voltage fluctuation is also eliminated. This paper proceeds as follows. Section 2 identifies similar works on display backlighting. Section 3 discusses the proposed technique and the simulation results are analyzed in Section 4. The conclusion of the paper is presented in Section 5.

2. Related works

Various types of SIMO topology-based boost converters are used to achieve uniform current distribution to all channels [8–13]. An extended source-based direct LED display backlighting technique was used to provide uniform current [14]. An auto-zeroed integrator-based accurate current control technique was implemented to provide uniform current with better power efficiency [15]. A dual mode current control with dimming control and current balancing was designed and used for display backlighting applications [16]. A feedback reversing technique with extended resources for uniform illumination for directly lit backlighting was tested [17]. An improved uniform dimming with fast response time for an eight-channel LED driver was designed and analyzed for backlighting [6]. A single time-shared control loop-based SIMO dimmable LED driver with uniform current distribution was discussed [4]. A digitally controlled boost LED driver for low power display backlighting was exhibited [18]. The use of DC/DC drivers in an active power distribution management application for electric vehicles was illustrated [19]. Frequency modulation (FM) technique-based EMI reduction was proposed [20].

A SIMO-based LED driver using a current balancing technique is shown in Figure 2. The SIMO boost converter-based LED driver drives three channels with individual channel current of 300 mA and supply voltage of 12 V. As soon as the LED driver is switched ON, the inductor in the boost converter is charged. During the ON time of the square wave, current is allowed to flow, which is driving the gate terminal of transistor S_M . During the OFF time of the gate driving, transistor S_M is in cut-off state and the total current through the inductor is supplied to the first channel through transistor S_1 . The same thing is repeated to the second and third channels by S_2 and S_3 , respectively. This SIMO-based boost converter is designed to work in continuous conduction mode and it supplies the total current to all three channels one by one in one switching period. The SIMO boost converter presented in [8] has a timing diagram as shown in Figure 3. In each switching period of the boost converter, one additional unwanted switching is present in the existing LED driver. The unwanted switching is repeated every $10.66 \mu\text{s}$ since the switching frequency of the existing LED driver is 93.75 kHz. The unwanted switching activities are circled in red color. For example, if the existing LED driver is operated for 1 h, it causes about 3.38×10^8 unwanted switching activities. The unwanted switching sequence in the existing LED driver dissipates one $\text{CV}^2 f \alpha$ J of energy per switching cycle. For 1 h of operation, it dissipates $3.38 \times 10^8 \times C \times V^2 \times f \times \alpha$ J of energy. Here C represents the load capacitance, V represents the supply voltage, f represents the frequency of operation, and α represents the switching activity. This unwanted additional switching in each switching period causes an enormous amount of dynamic power dissipation in the existing LED driver, which in turn will heat the system and a thermal runaway situation may occur. The unwanted additional switching sequences are completely eliminated by a novel switching technique in the proposed low-power LED driver for display back light applications.

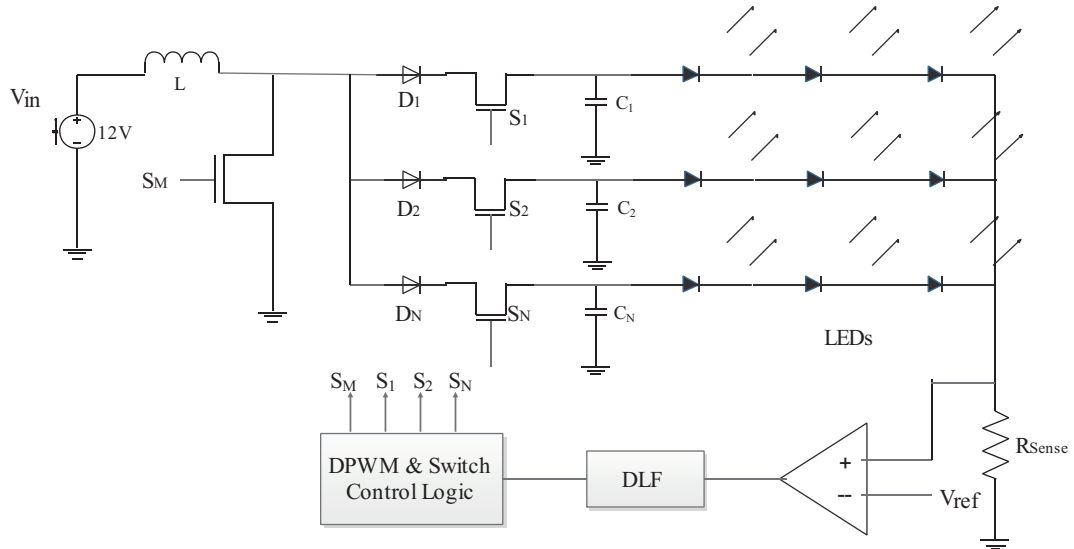


Figure 2. SIMO boost converter topology [8].

3. Proposed work

A single-inductor eight-channel low-power LED driver for portable display backlight applications is proposed in this paper. A SIMO DC-DC boost converter is used in this work. Figure 4 exhibits the timing diagram of the proposed design. The timing diagram exhibits the switching transitions of the power transistor of boost converter T_{BC} and all control transistors of all eight channels from T_1 to T_8 . Time multiplexing-based uniform current distribution to all eight channels is implemented in the proposed work. While the switching transistor

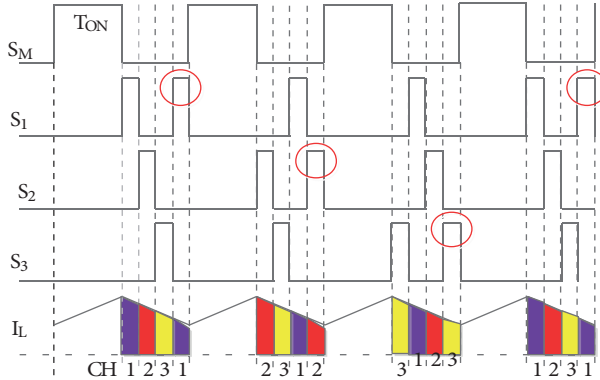
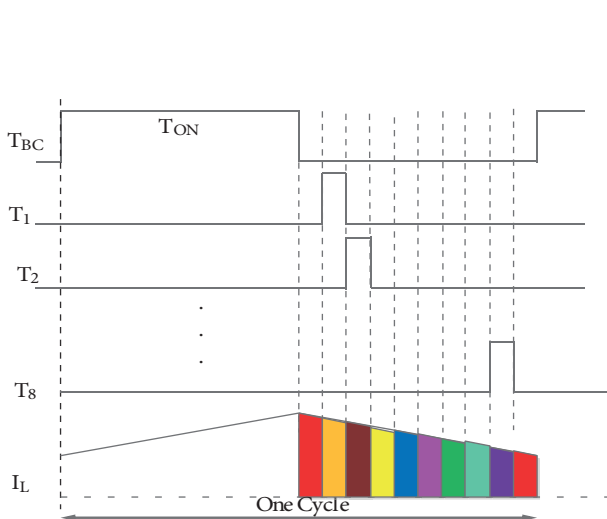
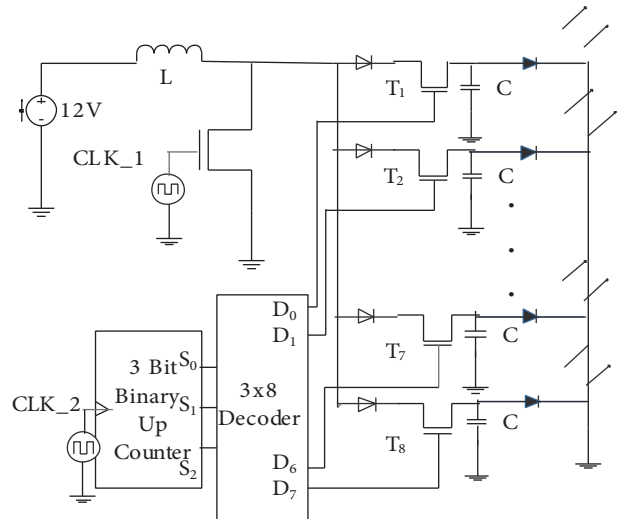


Figure 3. Timing diagram of time division multiplexed control [8].

of boost converter T_{BC} is in the ON state, the inductor is charged to the maximum current of 300 mA. During the OFF state of transistor T_{BC} , this total current is distributed to all eight channels one by one in a time-multiplexing manner. Since the currents in all channels are almost equal, the proposed system has minimum current balancing error and uniform brightness is achieved in the display panel, which in turn provides better picture clarity. The proposed boost converter uses 93.75 kHz as its switching frequency for comparing the performance metrics of the proposed LED driver with the existing LED driver. The time period of one cycle is 10.66 μ s. Hence, switching transistor T_{BC} is ON for 5.33 μ s and OFF for 5.33 μ s. During the ON time of 5.33 μ s, the inductor is charged and it delivers a total current of 300 mA to the channels. During the 5.33 μ s of OFF time of switching transistor T_{BC} , the current delivered by the inductor is uniformly distributed to all eight channels based on time-multiplexing. The total current of 300 mA is provided to each channel for 0.3 μ s. Transition or changeover time of 0.1 μ s is provided between each channel in a cycle. A guard time of 1.1 μ s is provided before starting the switching sequences of the channels and 1.1 μ s is allocated after completing current distribution to all eight channels. This eliminates the unwanted glitches in the proposed LED driver, whereas in the existing LED driver [8], the current is distributed to consecutive channels by switching OFF transistor S_1 of the first channel and switching ON transistor S_2 of the second channel simultaneously. This simultaneous ON and OFF transition of the control transistors of the channels causes glitches in the existing LED driver, which in turn consumes more power, and the distributed currents will not be uniform. The changeover time between the channels in the proposed system avoids simultaneous transitions and hence the unwanted glitches are completely eliminated. The control sequence for the control transistors of the channels were generated by a complex DPWM and digital loop filter [8]. This consumes a large area and enormous dynamic power because of unwanted switching transitions occurring in each cycle. Moreover, PWM causes EMI and unwanted noise and other side effects for the existing LED driver.

The switching transistors in the proposed LED driver are controlled by the switching pattern generated by a 3×8 decoder, which is driven by a 3-bit binary up-counter. The power transistor of the single-inductor eight-channel boost converter is switched at the same frequency [8] to compare the performance metrics of the proposed design. Output lines of the 3-bit binary up-counter are connected to the input terminals of the 3×8 decoder. The output lines of the 3×8 decoder are connected to the gate terminals of the control transistors of each channel. The schematic diagram of the proposed glitch and EMI-free low-power LED driver is shown in Figure 5. The 3-bit binary up-counter generates the required 3-bit binary combinations from '000' to '111', which in turn drives the 3×8 decoder.

**Figure 4.** Timing diagram of the proposed LED driver.**Figure 5.** Schematic diagram of the proposed low-power LED driver.

The clock frequency of the 3-bit binary up-counter is set to 1.5 MHz, which is 16 times faster than the switching frequency of power transistor T_{BC} in the boost converter. This generates the required switching pattern. The status of each channel in a cycle is represented in Table 1. In the first clock of the 3-bit counter, the first channel of the LED driver is switched ON by applying binary ‘1’ to the gate of nMOS transistor T₁. Similarly, in the consecutive clock cycles of the counter, the remaining channels are switched sequentially by transistors T₂–T₈. The average currents in all eight channels will have a relation as follows: I_{LED1} > I_{LED2} > I_{LED3} > I_{LED4} > I_{LED5} > I_{LED6} > I_{LED7} > I_{LED8}, since the channels of the LED driver are switched ON only during the decaying transient of the inductor current. Hence, the first channel will get the maximum current and the last channel will get the minimum current.

Table 1. Status of the individual channels of the proposed LED driver.

Clock	Present state	Next state	Status of individual channel							
			Ch1	Ch2	Ch3	Ch4	Ch5	Ch6	Ch7	Ch8
1	000	001	ON	OFF						
2	001	010	OFF	ON	OFF	OFF	OFF	OFF	OFF	OFF
3	010	011	OFF	OFF	ON	OFF	OFF	OFF	OFF	OFF
4	011	100	OFF	OFF	OFF	ON	OFF	OFF	OFF	OFF
5	100	101	OFF	OFF	OFF	OFF	ON	OFF	OFF	OFF
6	101	110	OFF	OFF	OFF	OFF	OFF	ON	OFF	OFF
7	110	111	OFF	OFF	OFF	OFF	OFF	OFF	ON	OFF
8	111	000	OFF	OFF	OFF	OFF	OFF	OFF	OFF	ON

Each channel is switched only one time in a cycle, which avoids the unwanted additional switching, whereas in the existing LED driver [8] an additional unwanted switching occurs in each switching cycle of the boost converter, which dissipates additional dynamic power as heat. The existing LED driver consumes total power of 12.4 W, whereas the proposed low-power LED driver consumes total power of 8.746 W since the

glitches and the additional switching activities are completely eliminated. Hence, the proposed low-power LED driver outperforms the existing LED driver.

4. Results and discussion

The proposed single-inductor eight-channel low-power LED driver is designed and implemented in the 180-nm CMOS process. Simulation parameters used in this proposed work are listed in Table 2. The proposed LED driver is simulated using the Cadence Virtuoso Analog Design Environment (ADE) platform with Spectre as the simulator. Transient analysis and DC analysis are performed at the temperature of 27 °C to validate the proposed design. The inductor current of the SIMO LED driver is shown in Figure 6. The average inductor current is 302.57 mA. Inductor current reaches a stable state after 100 μ s. The inductor is charged every 5.33 μ s and similarly discharged every 5.33 μ s since the frequency of operation of the boost converter is 93.75 kHz with a time period of 10.66 μ s. The design value of the inductor is 1 mH and the supply voltage is 12 V. Figure 7 exhibits switching pulses of the boost converter and the individual channels. During OFF times of the switching pulse of the boost converter all eight channels are switched sequentially one by one by applying the concerned switching patterns to the control transistors T₁–T₈ from the 3 × 8 decoder, which is driven by a 3-bit binary up-counter. The counter changes its states every 0.66 μ s, which generates the required pattern to control the channels by the decoder. Since the unwanted switching activities are eliminated, the proposed LED driver consumes a total power of 8.746 W when the supply voltage is 12 V and the temperature is 27 °C with frequency of operation of the boost converter of 93.75 kHz. The individual currents are exhibited in Figure 8. The first channel gets the maximum current of 304 mA, whereas the eighth channel gets the minimum current of 299.4 mA. The individual channel currents for one cycle are shown in Figure 9. The current balancing error in each channel with corresponding individual channel currents are listed in Table 3. The maximum current balancing error of the proposed LED driver is 0.775%, minimum current balancing error is 0.019%, and average current balancing error is 0.451%, whereas the maximum current balancing error of the existing LED driver is 2.04% and the minimum balancing error is 0.12%. The prototype of the proposed single-inductor 8-channel LED driver, which is controlled by the Xilinx Spartan-6 FPGA board, is depicted in Figure 10. The LED array has 8 channels or strings of LEDs with 9 LEDs in a string for a total of 72 LEDs in the display panel. These 8 channels or strings are controlled by the digital circuits such as a 3-bit binary up-counter and 3 × 8 decoder

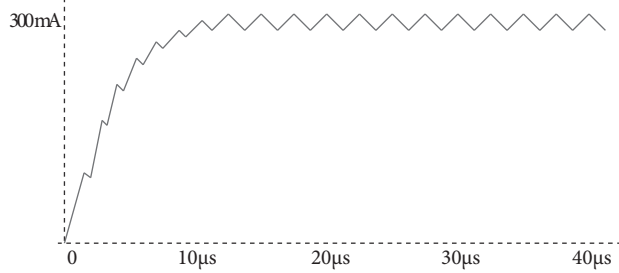


Figure 6. Inductor current of the proposed LED driver.

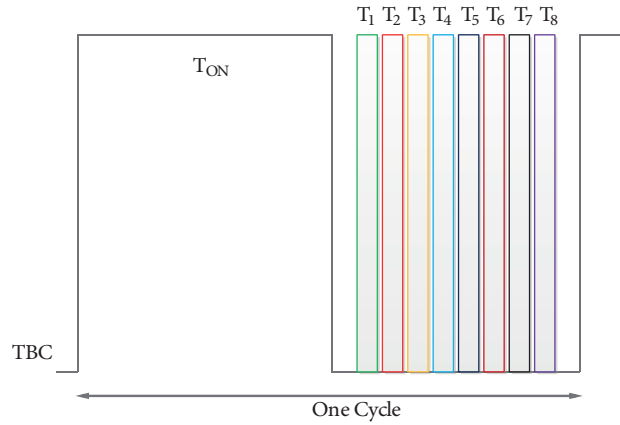


Figure 7. Control pulses to individual channel in the proposed LED driver.

modules. These digital circuits are implemented in the Xilinx Spartan-6 FPGA board. The total current is uniformly distributed to all channels or strings of LEDs in a time division multiplexing manner by the proposed system so that the proposed LED driver can be used for larger displays. The list of components used in the prototype of the proposed LED driver are displayed in Table 4. The prototype of the proposed LED driver has been realized as hardware.

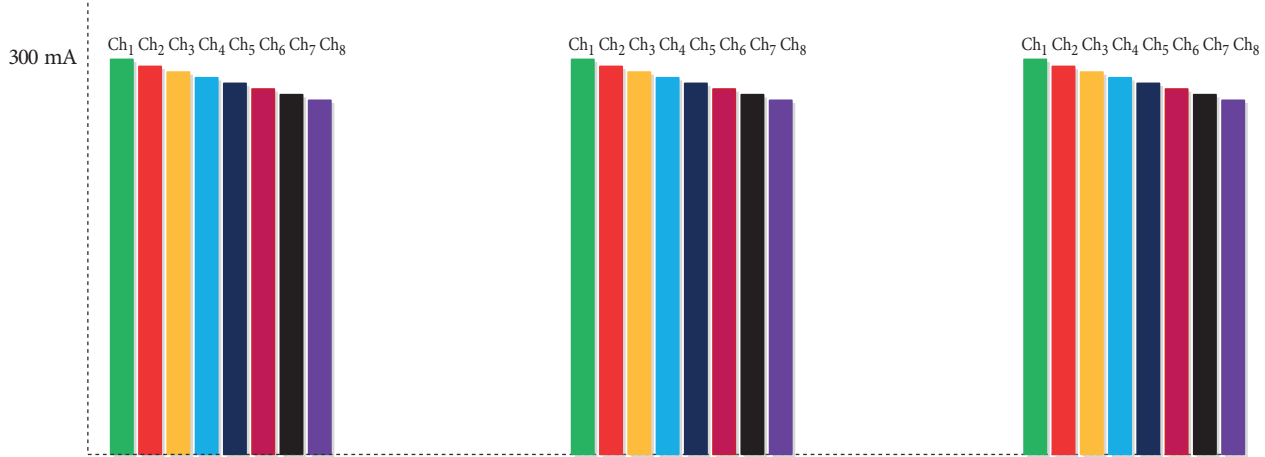


Figure 8. Individual channel currents of the proposed LED driver.

The comparative analysis of the experimental results of the proposed and existing LED drivers are listed in Table 5. The existing and proposed LED drivers were designed to deliver a current of 300 mA to each channel with supply voltage of 12 V and switching frequency of 93.75 kHz. The experimental verification of the synchronization between CLK1 (switching pulse of power MOSFET T_{BC}) and CLK2 (switching pulses of MOSFETs $T_1 - T_2$) has been performed using CRO, which is exhibited in Figure 11. The number of channels present in the existing LED driver is three, whereas the proposed LED driver has eight channels. The Spartan-6 FPGA kit consumes 0.576 W of power. The proposed LED driver has peak power efficiency of 96.26% without the Spartan-6 FPGA kit and 89.92% with the FPGA kit. The peak power efficiency of the existing LED driver without the PSoC kit is 93% and it is 85.6% with the PSoC kit.

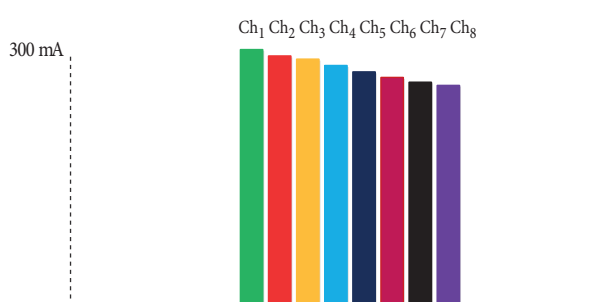


Figure 9. Individual channel currents in one switching cycle.

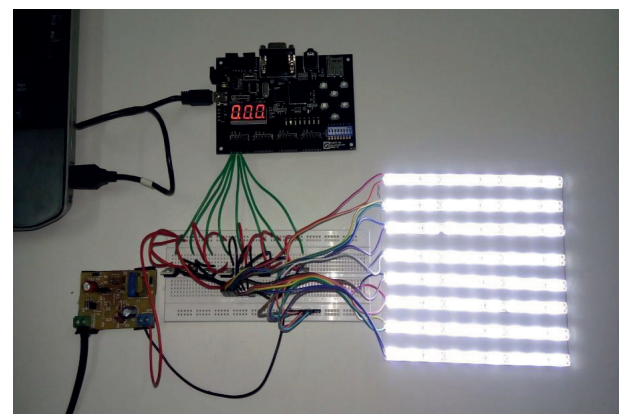


Figure 10. Prototype of the proposed single-inductor 8-channel LED driver, controlled by the Xilinx Spartan-6 FPGA board.

Table 2. Simulation parameters.

Simulation tool	Cadence Virtuoso ADE
Technology	GPDK 180 nm
Switching frequency	93.75 kHz
Counter clock frequency	1.5 MHz
Supply voltage	12 V
Temperature	27 °C
Analysis	Transient
Inductor (L)	1 mH
Capacitor (C)	10 μF

Table 3. Individual channel currents and current balancing error.

Currents	Value (mA)	Average current = 301.66 mA difference current (mA)	Current balancing error (%)
I _{ch1}	304	2.34	0.775
I _{ch2}	303.3	1.64	0.543
I _{ch3}	302.7	1.04	0.344
I _{ch4}	302.1	0.44	0.145
I _{ch5}	301.6	0.06	0.019
I _{ch6}	300	1.66	0.550
I _{ch7}	300.2	1.46	0.483
I _{ch8}	299.4	2.26	0.749

Table 4. List of components used in the prototype of the proposed LED driver.

Device	Part number	Description
Spartan-6 FPGA	XC6SLX9	Mimas V2 Spartan 6 FPGA Development Board with DDR SDRAM
Switches	IRF 540	N-channel Trench MOS transistor, 100 V, 22 A
Inductor	24S100C	1 mH, 1.6 A
Capacitor	106TTA050M	10 μF, 50 V
Diodes	DB22320	Schottky, 30 V, 1.5 A
Gate driver	FAN7382	Monolithic half-bridge gate driver IC
LEDs	CITRA GHH8987GV	White LED strip lights

5. Conclusion

A novel decoder-based digitally controlled single-inductor eight-channel low-power LED driver for display backlight applications has been presented in this paper. The switching sequences were generated by the 3-bit binary up-counter and the 3×8 decoder. Unwanted switching activities are completely removed in the

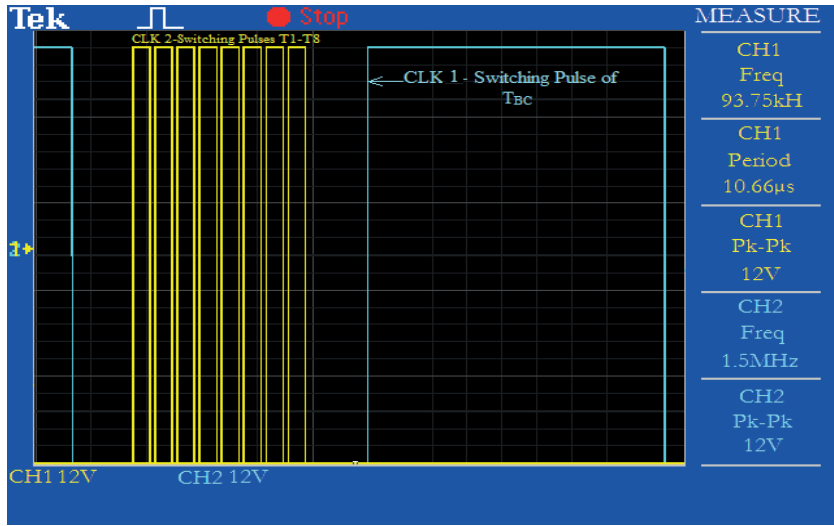


Figure 11. Experimental verification: synchronization of CLK1 and CLK2 (switching pulses of T_{BC} (CLK1) and $T_1 - T_8$ (CLK2)).

Table 5. Comparative analysis of measured experimental results.

Parameter	[8]	Proposed work
Input voltage	9–12 V	12 V
Switching frequency	93.75 kHz	93.75 kHz
Output voltage	16–23 V	24 V
Max. LED current/channel	300 mA	300 mA
No. of channels	3	8
Peak efficiency	93% w/o PSoC 85.6% with PSoC	96.26% w/o FPGA 90.13% with FPGA
Max. current balancing error	2.04%	1.33%
Min. current balancing error	0.12%	0.019%
Average current balancing error	-	0.451%

proposed LED driver, which in turn optimizes the dynamic power consumption. The proposed LED driver consumes total power of 8.746 W when the simulation is performed at 27 °C with the frequency of operation of the boost converter set to 93.75 kHz, whereas the existing LED driver consumes total power of 12.4 W. The proposed LED driver is designed to deliver current of 300 mA to each channel and the average current is 301.66 mA, which results in maximum current balancing error of 0.775% in the proposed design whereas the maximum current balancing error of the existing LED driver was 2.04%. Minimum current balancing errors of the proposed and existing LED drivers are 0.019% and 0.12%, respectively. The proposed LED driver has peak power efficiency of 96.26% without the Spartan-6 FPGA kit and 89.92% with the FPGA kit, whereas the peak power efficiency of the existing LED driver without the PSoC kit is 93% and it is 85.6% with the PSoC kit. Hence, the proposed decoder-based low-power LED driver with novel switching scheme outperforms the existing LED driver.

References

- [1] Hong SI, Han JW, Kim DH, Kwon OK. A double-loop control LED backlight driver IC for medium-sized LCDs. In: IEEE 2010 International Solid-State Circuits Conference; 7–11 February 2010; San Francisco, CA, USA. New York, NY, USA: IEEE. pp. 116-117.
- [2] Doshi M, Zane R. Digital architecture for driving large LED arrays with dynamic bus voltage regulation and phase shifted PWM. In: IEEE 2007 Applied Power Electronics Conference and Exposition; 25 February–1 March 2007; Anaheim, CA, USA. New York, NY, USA: IEEE. pp. 287-293.
- [3] Lee ATL, Sin JKO, Chan PCH. Scalability of quasi-hysteretic FSM-based digitally controlled single-inductor dual-string buck LED driver to multiple strings. *IEEE T Power Electron* 2014; 29: 501-513.
- [4] Chen H, Zhang Y, Ma D. A SIMO parallel-string driver IC for dimmable LED backlighting with local bus voltage optimization and single time-shared regulation loop. *IEEE T Power Electron* 2012; 27: 452-462.
- [5] Hu Y, Jovanovic MM. LED Driver with self-adaptive drive voltage. *IEEE T Power Electron* 2008; 23: 3116-3125.
- [6] Hsieh YT, Liu BD, Wu JF, Fang CL, Tsai HH, Juang YZ. A high dimming-ratio LED driver for LCD backlights. *IEEE T Power Electron* 2012; 27: 4562-4570.
- [7] Hasan J, Ang SS. A high-efficiency digitally controlled RGB driver for LED pixels. *IEEE T Ind Appl* 2011; 47: 2422-2429.
- [8] Kim HC, Yoon CS, Jeong DK, Kim J. A single-inductor, multiple-channel current-balancing LED driver for display backlight applications. *IEEE T Ind Appl* 2014; 50: 4077-4081.
- [9] Shen Z, Chang X, Wang W, Tan X, Yan N, Min H. Predictive digital current control of single-inductor multiple-output converters in CCM with low cross regulation. *IEEE T Power Electron* 2012; 27: 1917-1925.
- [10] Huang MH, Chen KH. Single-inductor multi-output (SIMO) DC-DC converters with high light-load efficiency and minimized cross-regulation for portable devices. *IEEE J Solid-St Circ* 2009; 44: 1099-1111.
- [11] Kim J, Kim DS, Kim C. A single-inductor eight-channel output DC-DC converter with time-limited power distribution control and single shared hysteresis comparator. *IEEE T Circuits-I* 2013; 60: 3354-3367.
- [12] Ma D, Ki WH, Tsui CY, Mok PKT. Single-inductor multiple-output switching converters with time-multiplexing control in discontinuous conduction mode. *IEEE J Solid-St Circ* 2003; 38: 89-100.
- [13] Le HP, Chae CS, Lee KC, Wang SW, Cho GH, Cho GH. A single-inductor switching DC-DC converter with five outputs and ordered power-distributive control. *IEEE J Solid-St Circ* 2007; 42: 2706-2714.
- [14] Kuo SH, Chen CF. Design of direct LED backlighting based on an analytical method of uniform illumination. *J Disp Technol* 2016; 99: 1-8.
- [15] Lim BM, Ko YH, Jang YS, Kwon OH, Han SK, Lee SG. A 200V 98.16% efficiency buck LED driver using integrated current control to improve current accuracy for large scale single-string LED backlighting applications. *IEEE T Power Electron* 2016; 31: 6416-6427.
- [16] Lin YL, Chiu HJ, Lo YK, Leng CM. LED backlight driver circuit with dual-mode dimming control and current-balancing design. *IEEE T Ind Electron* 2014; 61: 4632-4639.
- [17] Wu D, Wang K, Chigrinov VG. Feedback reversing design method for uniform illumination in LED backlighting with extended source. *J Disp Technol* 2014; 10: 43-48.
- [18] Oh TJ, Cho A, Ki SL, Hwang IC. A low-power and low-cost digitally-controlled boost LED driver IC for backlights. In: IEEE 2012 Asian Solid-State Circuits Conference; 12–14 November 2012; Kobe, Japan. New York, NY, USA: IEEE. pp. 237-240.
- [19] Alagöz BB, Keleş C, Kaygusuz A, Kaplan Y, Karabiber A. Power regulated DC/DC driver design by hierarchical control. *Turk J Elec Eng & Comp Sci* 2016; 24: 1325-1339.
- [20] Çabuk G, Kılımcı S. Reducing electromagnetic interferences in flyback AC-DC converters based on the frequency modulation technique. *Turk J Elec Eng & Comp Sci* 2012; 20: 71-86.

An efficient algorithm for computer tomography in low radiation images

B.S. Sathishkumar^{1*}, G. Nagarajan²

¹ Department of ECE, Research Scholar, Pondicherry University, Pondicherry Engineering College, Pondicherry, India

² Department of ECE, Professor, Pondicherry University Pondicherry Engineering College, Pondicherry, India

Corresponding Author Email: bssathishkumar.79@gmail.com

https://doi.org/10.18280/ama_a.610403

Received: 9 June 2018

Accepted: 15 October 2018

Keywords:

computer tomography, fan beam tomography, image reconstruction, iterative algorithm, parallel beam tomography, radiation dose

ABSTRACT

Computer Tomography (CT) is one of the efficient imaging techniques employed in medical field for the past few decades. In CT Scanning, image quality has influenced by several factors like noise, slice thickness, minimum and maximum contrast resolution, radiation dose etc., Radiation dose is one among important and challenging issues taken to optimize the reconstruction algorithm in CT. The radiation dose is controlled by tube current*time product (mAs), pitch or table speed, slice thickness, beam energy (kVp) and number of patients. In this paper, Landweber algorithm is used to check the improvement in quality of image in low radiation dose. The projected algorithm is compared with existing iterative reconstruction algorithm in Test Phantom, Head image and Thorax image and shows better results. The proposed methods will be useful to optimize an iterative reconstruction algorithm with adequate level of quality in computer tomography.

1. INTRODUCTION

Computer Tomography is a superior imaging method which uses an ionizing radiation and algorithms to attain the sectional view of object with higher accuracy in the variety of disease entity. Due to the benefits ensured in CT, its usage in medical field is more distinguished with other imaging [1]. Major issues in CT are needed to minimize the X-ray radiation during the imaging procedures. Advantage of using dual tree complex wavelet transform is that instead of capturing the signal energy in different path [2]. Necessity of preprocessing methods are for image normalization and to increase the contrast for achieving accurate analysis [3]. Under the situation of scarcity of data in the target domain, the performance of the traditional agent simulation model tends to decrease. In this scenario, the useful knowledge in the source domain is extracted to guide the target domain learning to obtain more appropriate class information and agent simulation performance is an effective learning method [4].

The patient exposed in X-ray radiation which may create the biological effects like cancer hereditary effects and non-cancer effect like respiration diseases, stroke and digestive disorders. Radiation dose is challenging are in image quality and diagnostic accuracy [5]. Increasing the radiation dose may reduce the noise and improve the spatial resolution in the image. But it increases the risk to patients. While decrease the radiation dose may lead more noise and lack of diagnostic accuracy in CT [6]. CT produces more accuracy in image. Many procedures to reduce the radiation dose are followed while maintaining adequate quality of image in clinical task [7].

The result of dose reduction can be approached in two conditions: The first one is to appropriately define the target image quality for each specific diagnostic task. The second one, dose reduction is to improve some aspects of image

quality, such as reducing image noise which can then be implemented in order to allow radiation dose reduction [8]. This task can be performed by optimizing scanning techniques, improving the image reconstruction and data processing [9]. Radiation dose is derived in many ways. The scanner radiation output is represented by volume CT dose index ($CTDI_{Vol}$). Organ dose is the measure of radiation risk to the organ undergoing in CT. Radiation dose also depends on time and sex. Effective dose can be defined equivalent doses in tissues and organs [10].

The paper is organized as follows. The section II discuss about the previous related works in this area. Section III explains about the proposed methods of algorithm and other iterative algorithms. Section IV discuss about the simulation results and their interpretation. Section V concludes the work.

2. RELATED WORKS

There are many algorithms reported to improve the quality of image during reconstruction in case of normal and reduced dose level. Image reconstruction algorithm is one which is more active role in achieving good quality of image to extract the detailed information from image. Two major types of reconstruction methods are used in tomography. Analytical is a single step reconstruction and it is quite sophisticated in more projections with less error. Iterative algorithm has best solution in the case of less number of projections and also noisy. Fig: 1. shows the block diagram of image reconstruction technique. Although the considerable computational complexity and speed of iterative reconstruction algorithm, required more memory space and dealing with real time data are major challenging issues in practical implementations.

It is seen that real-world problems are tainted with uncertainty due to lack of knowledge, imprecision, vagueness

etc [11]. The sufficient conditions for determining the non-singular H-matrices were given by applying the theory of diagonally dominant matrix [12]. This article introduces its important theoretical foundations and classifies and summarizes the latest research progress of error-eliminating theories [13].

Many imaging strategies can reduce radiation dose while maintain appropriate diagnostic quality for the clinical task [14]. Dose Reduction Guidance (DRG) is an alternative tool to assist in building protocol that utilize Adaptive Statistical image Reconstruction (ASiR) to reduce the MAs needed for scan acquisition [15].

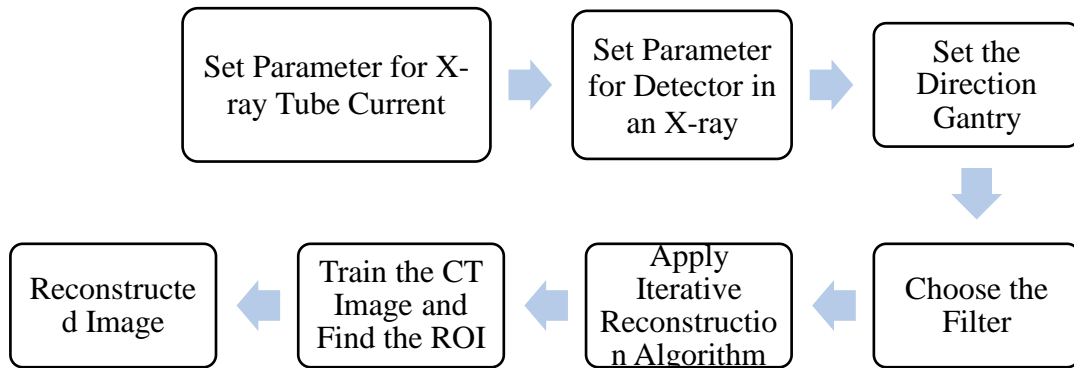


Figure 1. Block diagram of image reconstruction technique

Aaron Sodickson [16], demonstrated the hardware and software available to appropriate quality in a radiation exposure for the clinical scenario. In CT, Artifacts have different from noise, beam hardening, scattering, motion, helical, ring, etc., F. E. Boas, et al., [17] presented the reduction of artifacts and methods to avoid the artifacts in tomography. CT scanners used to create cross-sectional images through attenuation properties from different directions. The author [18] proposed radiation reduction strategies without compromising the quality of reconstructed image. Huaiqun Guany, et al., [19] made a survey on various projections methods in the computer tomography were described.

The two aspects of a contradiction exist in the same system and can mutually transform under certain conditions [20]. It focuses on hiding secret messages inside a cover medium [21]. All of the techniques discussed are reversible information embedding techniques in the spatial domain [22]. This paper presents an approach to simplify the feature extraction method to identify varying character patterns [23].

Various dose reduction and patient movements during inspections are investigated in tomography [24-25]. W. C. Scarfe, et al., [26] presents developments and usage of the cone beam in clinical applications. CBCT is an accurate image modality in normal and reduced radiation dose in proving the quality of image. Also, the future enhancement in CBCT is presented like reducing scan time, provide multimodal imaging and improving image fidelity. [27] Described the mathematical and benefits of radon transform in the development of image reconstruction in CT image.

2.1 Dose reduction stratégies

The quality of image is highly suffered by noise and inversely related to radiation energy. This shows that the dose reduction is important while try to reduce patient dose, image quality should not be compromised. The challenge is in finding a balance between dose and noise that allows the

images to be of diagnostic quality while utilizing the lowest dose possible. Noise (specifically, quantum noise) is generally characterized by graininess on image. The way to reduce the noise is to increasing the radiation dose. Since radiation dose is inversely proportional to image noise. In other words, noise is inversely related to the number of X-rays (which are proportional to mAs) used to create the image by the following relationships (assuming all other parameters are kept constant):

$$\text{Noise} \propto \frac{1}{\text{Number of } x\text{-rays}} \propto \frac{1}{\text{mAs}} \propto \frac{1}{\text{Radiation Dose}} \quad (1)$$

Hence the selection of optimal parameters in the dose reduction is needed. Dose reduction parameters are classified as follows in Fig. 2.

- Scanning Parameters
- Anatomical Parameters
- Technical Parameters

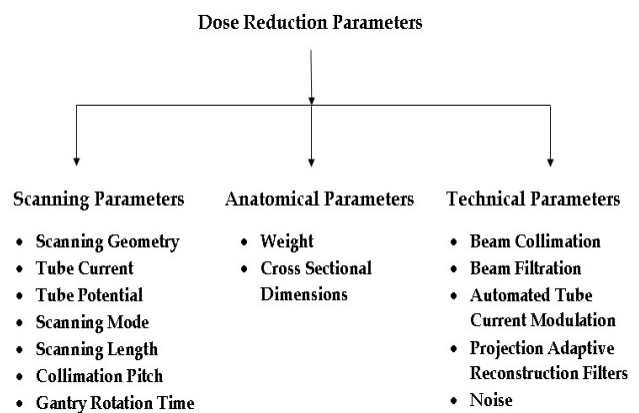


Figure 2. Clasificación de dose reduction

3. PROPOSED ALGORITHM

This work is to implement an efficient algorithm for computer tomography in low radiation CT images. There are many efforts and investigate in improvement in quality of image, technology and image reconstruction algorithm to achieve the tradeoff between image quality and radiation dose. There are many efforts have been taken on suitable utilization and safety of CT scanning to make the better quality of image in reducing the radiation dose. There are more efforts and investigations in improvement in quality of image, technology and image reconstruction algorithm to achieve the tradeoff between image quality and radiation dose.

3.1. Reconstruction algorithms

Image reconstruction is aided to improve the differentiation of contrast. The number of projections is fixed to reduce dose level and scanning time to the patient and then the information received from the projections improved by high performance reconstruction algorithm. The varieties of algorithms are available to produce accurate reconstruction at the cost high computation time in CT. Some of the algorithms uses the prior knowledge about the object like number of different kind of materials, it characteristics and gray levels, etc., these parameters potentially effective in selection of the projections, increases the accuracy and significantly reduce the noise.

The Landweber algorithm for solving the system $Ax=B$ is

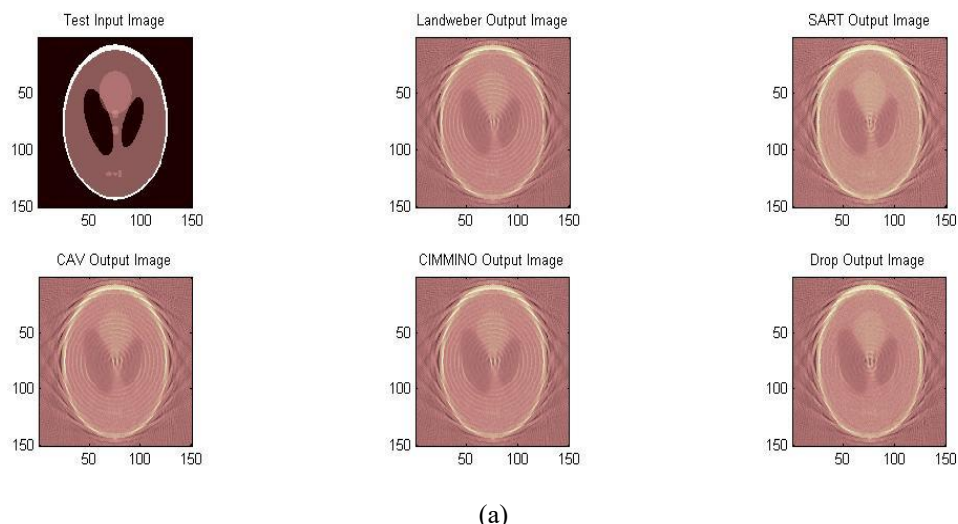
$$x^{k+1} = x^k + \gamma A^\dagger (b - Ax^k) \quad (2)$$

where, γ is a selection parameter, we can write the Landweber iteration as

$$x^{k+1} = Tx^k$$

$$Tx = (1 - \gamma A^\dagger A)x + A^\dagger b = Bx + b \quad (3)$$

The Landweber algorithm actually solve the square linear



system $A^\dagger A = A^\dagger b$ for a least-square solution of $Ax=B$ for the unique solution, of $Ax=B$, say \hat{x} the error at the k^{th} step is

$$e^k = \hat{x} - x^k \text{ and } B e^k = e^{k+1} \quad (4)$$

When there is multiple solution of $Ax=b$ the solution fixed by Landweber algorithm will be the one of the closest to the starting vector.

4. SIMULATION RESULTS

The proposed scheme is simulated in the MATLAB. The parameters like Correlation coefficient Vs number of iteration and Mean squared error Vs number of iterations are evaluated in reduced dose level in computer tomography performed through different iterative algorithms. The proposed landweber iteration algorithm and other iterative algorithms performance are compared in terms of SC, AD, MD, NAE, PSNR., etc. these parameters are found in parallel beam and Fan beam geometry arrangements.

To reduce the exposure of radiation to the patient in computer tomography, small number of projections has been explored. (e.g., projections restricted to a small region of interest). With small set of orientations, the tomographic image is reconstructed by algorithm like SART, DART, CAV, Cimmino and Landweber. Also set the parameters initially at the lower the tube current which inturn reduce the radiation exposure of less amount. The number of projections is taken as small. This gives an image which consists of fewer amounts of image details. The parameter such as Mean Absolute error and correlation coefficient are measured with different iteration in test image, head image and thorax image simulated through different iterative algorithms. The simulation is done to obtain the correlation coefficient versus number of iterations and Mean square error versus number of iteration curves are simulated for the reduced dose in parallel beam and fan beam type of computer tomography and compared with the different iterative algorithm. A MATLAB generated test phantom, Head CT and Thorax images are considered as input image and reconstructed image of different algoeithms for fixed number of projections and iteration shows in Figure 3.

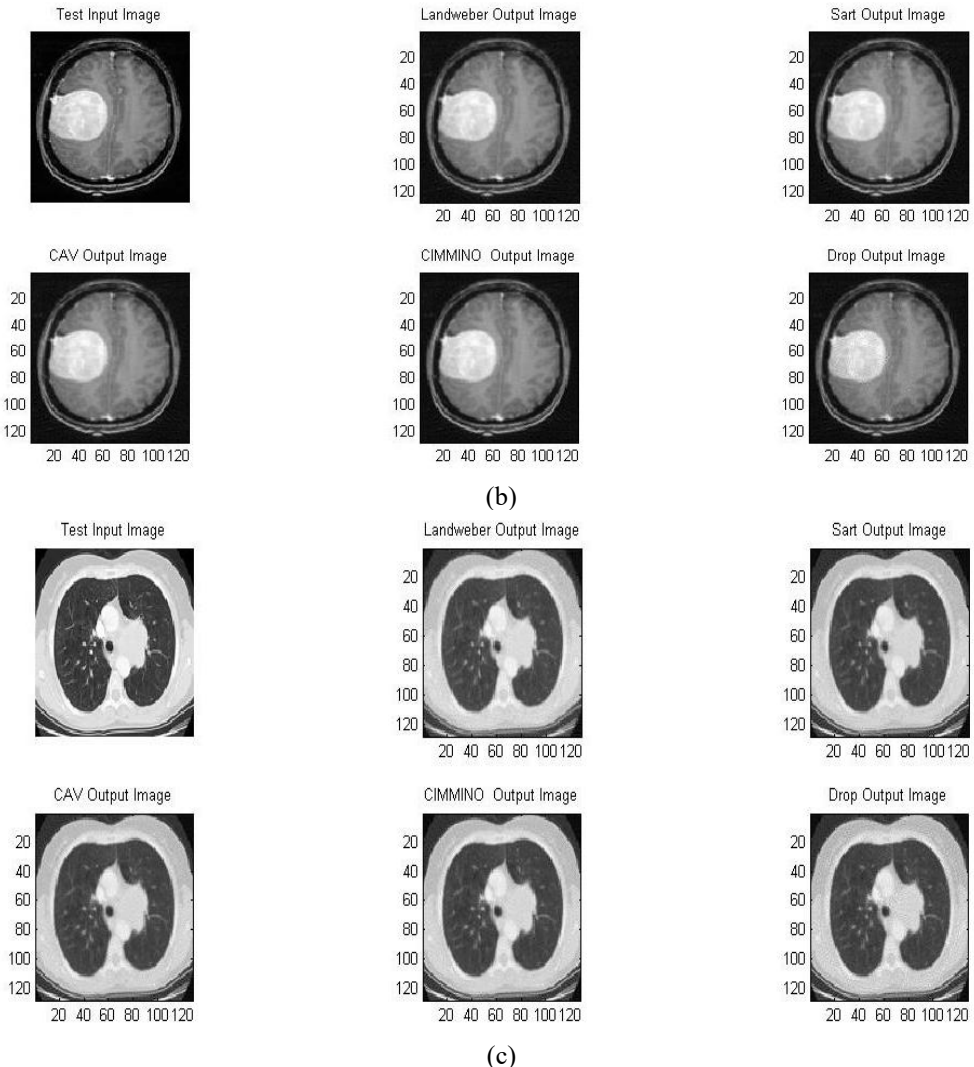


Figure 3. (a) Test Image and reconstructed image (b) Head image and reconstructed image (c) Thorax image and reconstructed image

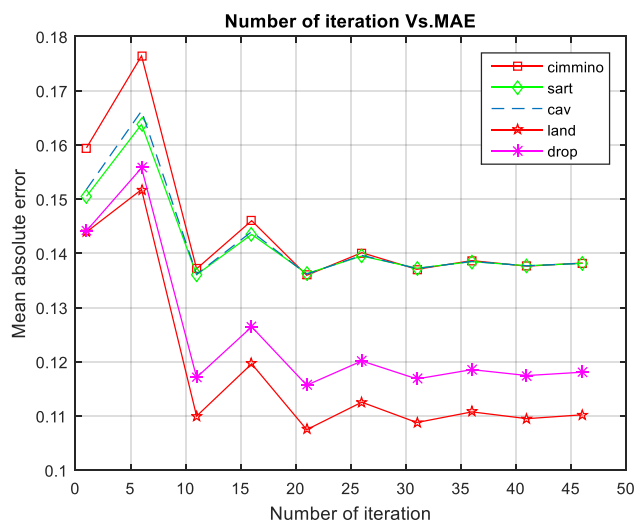


Figure 4. Mean absolute error between original and reconstructed image
(Parallel beam - test image)

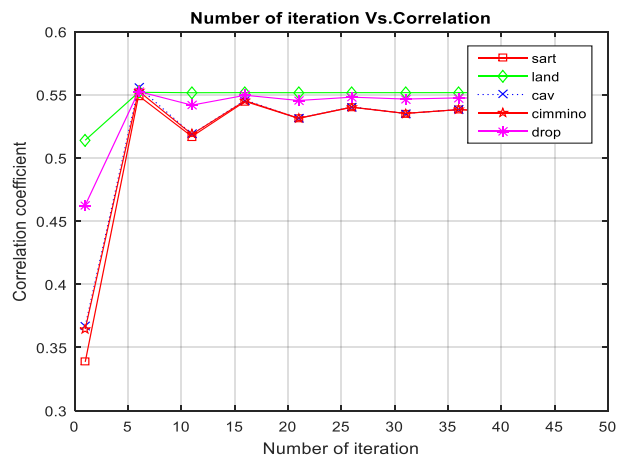


Figure 5. Correlation coefficient between original and reconstructed image
(Parallel beam- test image)

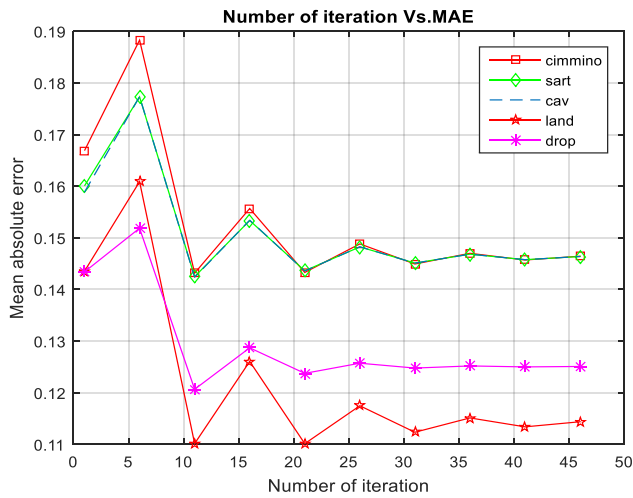


Figure 6. Mean absolute error between original and reconstructed image
(Fan beam - test image)

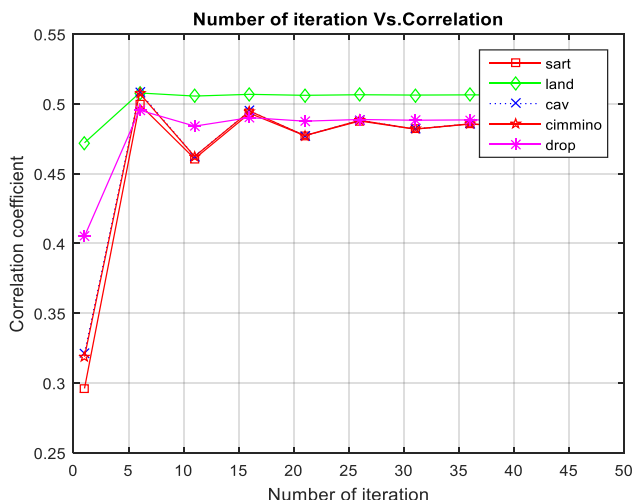


Figure 7. Correlation coefficient between original and reconstructed image
(Fan beam - test image)

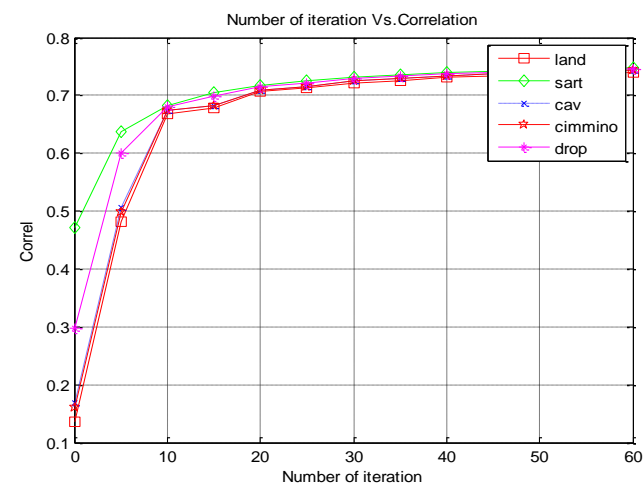


Figure 8. Correlation coefficient between original and reconstructed image
(Fan beam – head image)

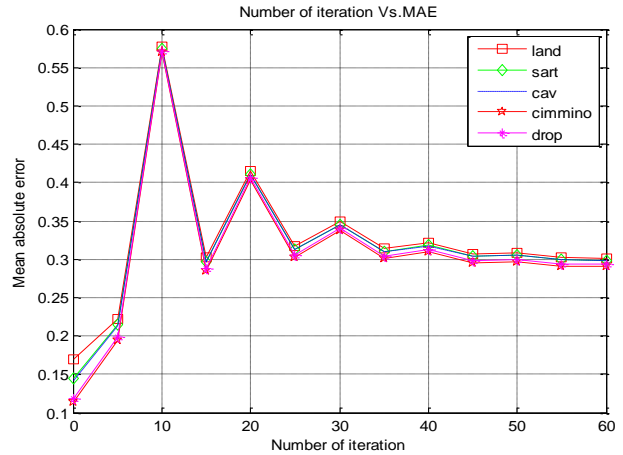


Figure 9. Mean absolute error between original and reconstructed image
(Fan beam – head image)

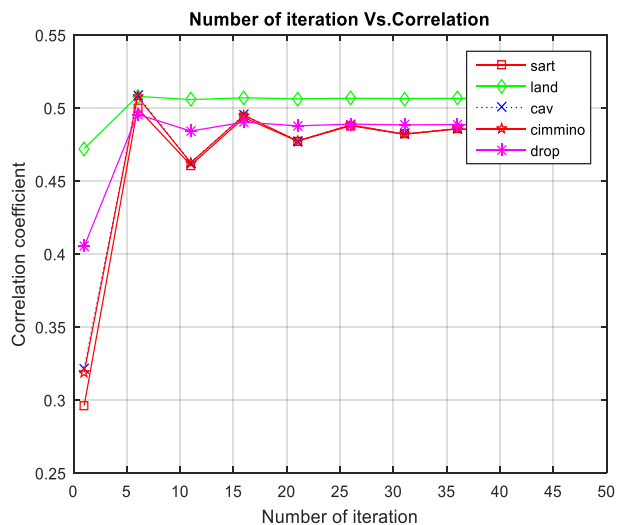


Figure 10. Correlation coefficient between original and reconstructed image
(Fan beam – thorax image)

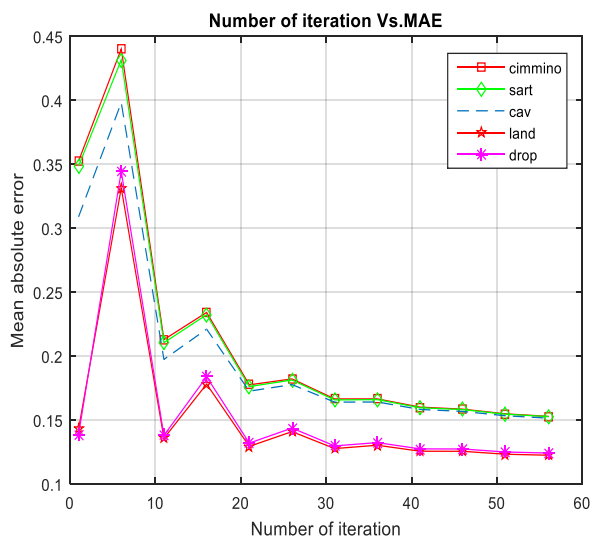


Figure 11. Mean absolute error between original and reconstructed image
(Fan beam – thorax image)

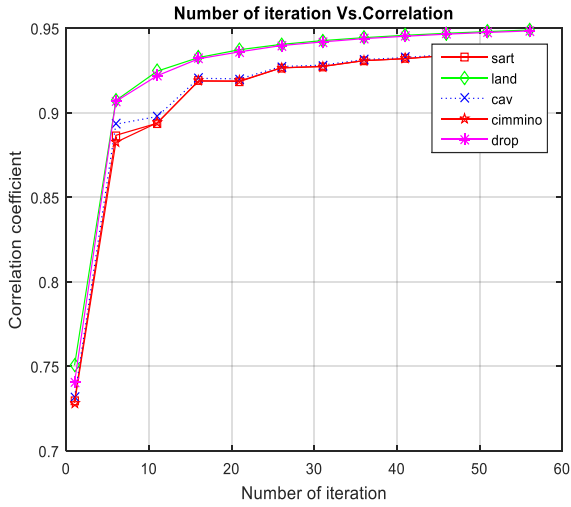


Figure 12. Correlation coefficient between original and reconstructed image
(Parallel beam – thorax image)

Figs. 4 to 7 show the performance comparison between proposed and other iterative algorithm. The mean square error and correlation coefficient are measured in original and reconstructed image for different iteration in Test phantom simulated with different iterative algorithms. The proposed landweber iteration algorithm produces much better results in

lower iteration itself with quality of image.

Figs. 8 and Fig. 9 show the performance comparison of head image configured in parallel beam and fan beam tomography simulated with iterative algorithms and plot the curves of the proposed and other iterative algorithms. It can be observed that the reconstructed image of the proposed method is better than other algorithms. As lower number of iteration, less error is obtained between the original and reconstructed image with fixed number of projections.

Fig. 10 to Fig. 12 illustrate the mean square error and correlation coefficient is measured in thorax image in parallel and fan beam tomography simulated by the proposed and existing iterative algorithms.

Table 1 below shows the measurement of image quality by simulating different iterative algorithms in the Test Phantom, Head Image and Thorax Image and parameters like Structural Content (SC), Absolute Difference (AD), Maximum Difference (MD), Normalized Absolute Error (NAE), Normalized Cross Correlation (NCC), Mean Absolute Error (MAE) and Peak Signal to Noise Ratio (PSNR) are calculated.

There have been many attempts in simulation were taken to produce the good quality of image in less number of projections and iterations. It is observed that the proposed algorithm called landweber iteration algorithm proved to be good in visual perception and error analysis compared to other algorithms.

Table 1. Performance of proposed scheme

Image / Parameters	Reconstruction Algorithm	SC	AD	NAE	MD	NCC	MAE	PSNR
Test Image Fan Beam	Landweber (Proposed)	2.18	0.014	0.884	0.995	0.488	0.98	9.636
	SART	1.899	0.037	0.857	0.962	0.500	1.0	9.616
	CAV	2.180	0.014	0.884	0.995	0.500	0.98	9.626
	CIMMNO	2.180	0.014	0.885	0.995	0.458	0.96	9.624
	DROP	1.963	0.003	0.884	0.991	0.489	0.96	9.626
Parallel Beam Image	Landweber (Proposed)	2.412	0.017	0.916	0.97	0.414	0.93	9.627
	SART	2.016	0.0780	0.890	0.93	0.466	0.06	9.626
	CAV	2.412	0.0177	0.917	0.94	0.467	0.07	9.624
	CIMMNO	2.413	0.0176	0.915	0.95	0.414	0.06	9.623
	DROP	2.101	0.087	0.916	0.96	0.449	0.06	9.625
Thorax Image	Landweber (Proposed)	2.100	0.035	1.098	238.418	0.99	0.121	78.936
	SART	2.101	0.032	1.098	238.431	0.399	0.120	78.935
	CAV	2.101	0.032	1.090	238.431	0.399	0.121	78.924
	CIMMNO	2.098	0.011	1.099	238.430	0.399	0.135	78.940
	DROP	2.104	0.080	1.099	238.394	0.399	0.140	78.996

5. CONCLUSION

Landweber based iterative reconstruction algorithm is implemented for computer tomography in parallel beam and cone beam to achieve the good quality of images in the reduced dose level in order to reduce the overall radiation exposure. The problems of imaging are dealt with the trade-off between data size, the image quality and the algorithm computational complexity to create the image in reduced dose level. In this paper, SART, CAV, CMMNO, DART and landweber iterative reconstruction algorithms are simulated in reduced dose level. The performances of execution are verified in terms of the quality of image. The reduction of dose is accomplished through drop off the tube current like 100 milli amps to 40 and 17 milli amps. The Landweber iterative reconstruction in the reduced dose level performs better image quality in different images.

REFERENCES

- [1] Magrini A, Lazzari S, Marenco L, Guazzi G. (2017). A procedure to evaluate the most suitable integrated solutions for increasing energy performance of the building's envelope, avoiding moisture problems. International Journal of Heat and Technology 35(4): 689-699. <https://doi.org/10.18280/ijht.350401>
- [2] Kim K, et al. (2015). Sparse-view spectral CT reconstruction using spectral patch-based low-rank penalty. IEEE Transactions on Medical Imaging 34(3): 748-760. <https://doi.org/10.1109/TMI.2014.2380993>
- [3] Navitha CH, Sivani K, et al. (2017). Adaptive wavelet transform based rake receiver for ultra-wideband systems. AMSE-IIETA Journals -Series: Advances B 60(2): 357-371.
- [4] Joshi S, Karule PT. (2018). Review of preprocessing techniques for fundus image analysis. AMSE-IIETA Journals-2017-Series: Advances B 60(2): 593-612.
- [5] Wei HC, Li XB. (2017). Agent simulation model based on similarity measure. AMSE-IIETA Journals -2017-Series: Advances D 60(4): 657-672.
- [6] McCollough CH, Primak AN, et al. (2009). Strategies for reducing radiation dose in CT. Radiological Clinical of North America 47(1): 27–40.
- [7] Ravenel JG, Leue WM, et al. (2008). Pulmonary nodule volume: Effects of reconstruction parameters on automated measurements - a phantom study. Radiology 247(2): 400–408.
- [8] Xu Q, Yu HY, et al. (2012). Low-dose x-ray CT reconstruction via dictionary learning. IEEE Transactions on Medical Imaging 31(9): 1682–1697. <https://doi.org/10.1109/TMI.2012.2195669>
- [9] Needell D, Tropp JA. (2009). Iterative signal recovery from incomplete and inaccurate samples. Applied and Computational Harmonic Analysis 26(3): 301–321.
- [10] Han X, Bian JG, et al. (2011). Algorithm-enabled low-dose micro-CT imaging. IEEE Transactions on Medical Imaging 30(3): 606–620. <https://doi.org/10.1109/TMI.2010.2089695>
- [11] Zambelli J, Bevins N, et al. (2010). Radiation dose efficiency comparison between differential phase contrast CT and conventional absorption CT. International journal of Medical Physics Letter 37: 2473-2479. <https://doi.org/10.1118/1.3425785>
- [12] Dutta P. (2017). Medical diagnosis via distance measures on picture fuzzy sets. AMSE Journals – AMSE IIETA publication-2017-Series: Advances A 54(2): 657-672.
- [13] Yang CY, Pan SP. (2017). New practical determination of non-singular h-matrices. AMSE JOURNALS-AMSE IIETA publication-Series: Advances A 54(2): 373-383.
- [14] Zhou J, Guo K, Ye S. (2015). The review of error-eliminating theories. AMSE JOURNALS-Series: Advances A 52(1):1-16.
- [15] Yu L, Liu X, et al. (2009). Radiation dose reduction in computed tomography: Techniques and future perspectives. Imaging in Medicine 1(1): 65–84. <https://doi.org/10.2217/iim.09.5>
- [16] Singh S, Karla MK, et al. (2011). Adaptive statistical iterative reconstruction techniques for radiation dose reduction in chest CT: A pilot study. Radiological Society of North America Journal 259(2) 565–573.
- [17] Sodickson A. (2013). Strategies for reducing radiation exposure from multidetector computed tomography in the acute care setting. Canadian Association of Radiologists Journal 64: 119-129.
- [18] Boas FE, Fleischmann D. (2012). CT artifacts: Causes and reduction techniques. IEEE Transaction on Medical Imaging 4(2): 29-240.
- [19] Peng H, Stark H. (1989). One step image reconstruction from incomplete data in computer tomography. IEEE Transaction on Medical Imaging 8(1): 16–31. <https://doi.org/10.1109/42.20358>
- [20] Guany H, Gordon R, et al. (1998). Combining various projection access schemes with the algebraic reconstruction technique for low-contrast detection in computed tomography. Physics of Medical and Biology 43: 2413–2421.
- [21] Zhou JG, Ye QX, et al. (2014). Error elimination based on error set. AMSE Journals –2014-Series: Advances A 51(1): 13-26.
- [22] Khamrui A, Mandal JK. (2014). A genetic algorithm based approach in image authentication using Z transform (GAIAZT). AMSE Journals- Series: Advances B 57(1): 20-30.
- [23] Ghosal SK, Mandal JK. (2014). Color image authentication based on two-dimensional separable discrete hartley transform (CIA2D-SDHT). AMSE Journals -Series: Advances B 57(1): 68-87.
- [24] Mandal RK, Manna N. (2014). Handwritten english character recognition using hoof segmentation of image matrix (HSIM). AMSE Journals -Series: Advances B 57(1): 88-107.
- [25] Aweda MA, Arogundade RA. (2007). Patient dose reduction methods in computerized tomography procedures: A review. International Journal of Physical Sciences 2(1): 001-009.
- [26] Cervinkova I, Walek P, et al. (2016). Possibilities of reducing radiation dose in computed tomography examinations in various age groups using an iterative model-based reconstruction technique. Pediatrics & Therapeutics 6(4): 2-7. <https://doi.org/10.4172/2161-0665.1000302>
- [27] Scarfe WC, Farman AG. (2008). What is cone-beam CT and how does it work? The Dental Clinics of North America 52: 707-730.
- [28] Toft PA, Sorensen JA. (1996). The radon transform – theory and implementation. kgs. Lyngby, Denmark:

NOMENCLATURE

Algorithm	A precise set of steps to be performed in a specific order to solve a problem. Algorithms are the basis for most computer programming.	Effective dose	A measurement, reported in Sv or rem, that attempts to account for the effects particular to the patient's tissue that has absorbed the radiation dose. It extrapolates the risk of partial body exposure to patients from data obtained from whole body doses to Japanese atomic bomb survivors. Although methods to calculate the effective dose have been established, they depend on the ability to estimate the dose to radiosensitive organs from the CT procedure. Also called effective dose equivalent.
Attenuation profile	The system accounts for the attenuation properties of each ray sum and correlates it to the position of the ray.		
Back projection	Process of converting the data from the attenuation profile to a matrix.		
Beam pitch	Table movement per rotation divided by beam width.	Effective slice thickness	Thickness of the slice that is actually represented on the CT image, as opposed to the size selected by the collimator opening. In traditional axial scanning, selected slice thickness is equal to effective slice thickness. However, because of the interpolation process used in helical scanning, the effective slice thickness may be wider than the selected slice thickness. Also called the slice-sensitivity profile.
Clinical information systems (CIS)	Information systems that keep track of clinical data. Collimators: Mechanical hardware that resembles small shutters and adjusts the opening based on the operator's selection.		
Computed tomography dose index (CTDI)	Dose reported to the FDA; slices must be contiguous.	Fan beam	The radiation emitted from the collimated x-ray source in single-detector row CT systems.
Computerized physician order-entry (CPOE)	System that electronically transmits clinician orders to radiology and other departments.	Focal spot	Area of the anode where the electrons strike and the x-ray beam is produced.
Cone beam	The radiation emitted from the collimated x-ray source in multidetector row CT systems.	Fourier transform (FT)	A method to study waves of many different sorts and also to solve several kinds of linear differential equations. Loosely speaking it separates a function into its frequency components.
CTDIvol	The CTDIvol is a measure of exposure per slice and is independent of scan length. It is the preferred expression of radiation dose in CT dosimetry.	Gantry	Ring-shaped part of the CT scanner that houses many of the components necessary to produce and detect x-rays
CTDIw	The CTDIw adjusts for variation across the scan field of view by providing a weighted average of measurements at the center and the peripheral slice locations (i.e., the x and y dimensions of the slice).	Gray scale	System that assigns a certain number of Hounsfield values to each shade of gray.
Detector	Element in a CT system that collects attenuation information. It measures the intensity of the transmitted x-ray radiation along a beam projected from the x-ray source to that particular detector element.	High attenuation	An x-ray beam is greatly impeded by an object; typically shown as light gray or white on an image.
Detector aperture	Size of the detector opening.	High-contrast resolution	Ability of a system to resolve, as separate forms, small objects that are very close together. Also call spatial resolution or detail resolution.
Detector array	Entire collection of detectors included in a CT system; detector elements are situated in an arc or a ring.	Image artifacts	Anything appearing on the image that is not present in the object scanned.
Detector efficiency	Ability of the detector to capture transmitted photons and change them to electronic signals.	Image reconstruction	Use of raw data to create an image.
Detector pitch	Table movement per rotation time divided by the selected slice thickness of the detector.	Isotropic	Equal in all directions; a voxel that is cube-shaped.
Detector spacing	Measured from the middle of one detector to the middle of the neighbouring detector; accounts for the spacing bar.	Kilovolt-peak (kVp)	Defines the quality (average energy) of the x-ray beam.
		Low attenuation	An x-ray beam that is nearly unimpeded by an object; typically shown as dark gray or black on an image.
		Matrix	Grid formed from the rows and columns of pixels.
		Milliampere (mA)	Measure of the tube current used in the production of x-ray energy. In conjunction with the scan time, it is the

Milliamperes-seconds (mAs)	quantitative measure of the x-ray beam. The product of millampere setting and scan time.	(ROI): Scan parameters	Factors that can be controlled by the operator and affect the quality of the image produced. These factors include milliamperes, scan time, slice thickness, field of view, reconstruction algorithm, and kilovolt-peak. When using helical scan methods, the operator also has a choice of pitch.
Nonuniform arrays	Detector rows that have variable widths and sizes. Also called adaptive or hybrid arrays.		
Organ dose	The estimated radiation dose to radio sensitive organs from CT procedures. These averages are used to calculate effective dose.		
Pitch	Relation of table speed to slice thickness. It is most commonly defined as the travel distance of the CT scan table per 360° rotation of the x-ray tube, divided by the x-ray beam collimation width.	Scan time	Time the x-ray beam is on for the collection of data for each slice. Most often it is the time required for the gantry to make a 360° rotation, although with over scanning and partial scanning options there may be some mild variation.
Radiation profile	Variations along the length, or z axis, of the patient; also referred to as the z-axis dose distribution.	Slice thickness	On a single-detector row system this is controlled by the width of the collimator opening. On a multidetector row system it is controlled by a combination of collimation and detector configuration.
Raw data	All measurements obtained from the detector array and sitting in the computer waiting to be made into an image. Also called scan data.	Spatial resolution	Ability of a system to resolve, as separate forms, small objects that are very close together. Also call high contrast resolution or detail resolution.
Ray	The path that the x-ray beam takes from the tube to the detector.	Threshold CT values	A predetermined CT value limit set by the operator in some types of 3D reformation techniques. The software will include or exclude the voxel depending on whether its CT number is above or below the threshold.
Ray sum	The detector senses each arriving ray and senses how much of the beam was attenuated.	Tube current	Measured in thousandths of an ampere, or milliamperes, it controls the quantity of electrons propelled from cathode to anode.
Reconstruction algorithm	Determines how the data are filtered in the reconstruction process. The appropriate reconstruction algorithm selection depends on which parts of the data should be enhanced or suppressed to optimize the image for diagnosis.	Uniform array	Detector rows that are parallel and of equal size.
Reference dose values	Values published by the ACR regarding the radiation dose that is acceptable for a variety of CT scans.	View	A complete set of ray sums.
Reference image	Displays the slice lines in corresponding locations on the scout image.	Voxel	Volume element. Three-dimensional cube of data acquired in CT.
Region of interest	An area on the image defined by the operator.	Z axis	Plane that correlates to the slice thickness, or depth, of the CT slice.

Tomographic image reconstruction using SART algorithm

B.S. Sathish Kumar*

Department of ECE,
Pondicherry Engineering College,
and
AVC College of Engineering,
Puducherry – 605 014, India
Email: bssathishkumar.79@gmail.com

*Corresponding author

G. Nagarajan

Department of ECE,
Pondicherry Engineering College,
Puducherry – 605 014, India
Email: nagarajanpec@pec.edu

Abstract: The rapid system and hardware development of X-ray computed tomography (CT) technologies has been accompanied by equally exciting advances in image reconstruction algorithms. The role of iteration reconstruction is widely used in many tomography applications. The use of iteration-based reconstruction algorithm offers more advantages than analytical methods. The development of algorithm can generally be classified into three major areas: analytical reconstruction, model-based iterative reconstruction and application-specific reconstruction. In this paper, the SART iteration-based reconstruction algorithm is simulated. Then the quality of the reconstructed image is expressed in terms of mean absolute error as compared to the original image. The simulation results are carried out using MATLAB tool. The performance comparisons are made using radon transform.

Keywords: image reconstruction; iteration algorithm; simultaneous algebraic reconstruction technique; SART; correlation coefficient; tomography.

Reference to this paper should be made as follows: Kumar, B.S.S. and Nagarajan, G. (2016) ‘Tomographic image reconstruction using SART algorithm’, *Int. J. Medical Engineering and Informatics*, Vol. 8, No. 3, pp.239–248.

Biographical notes: B.S. Sathish Kumar is a Research Scholar in Department of Electronics and Communication Engineering in Pondicherry Engineering College, Pondicherry, India. He received his BE in Electronics and Communication Engineering from Bharathidasan University and MTech from SASTRA University. He has more than 12 years of teaching experience and his area of interest include digital image processing, microprocessor and wireless communication. He has presented papers in various national and international conferences and journals. He is a life member of ISTE and BMI.

G. Nagarajan is currently working as a Professor and Head in Department of Electronics and Communication Engineering at Pondicherry Engineering College, Pondicherry, India. He has completed her post graduate and Bachelor degree in 1989 and 1996. To date he has authored nearly 50 research papers: 20 have been published in various reputed national and international journals and 30 have been presented and published in national and international conference proceedings. He serves as editorial board member in various journals. He is a life member of various professional bodies. He also serves as a doctoral committee member for faculty members pursuing PhD. He acted as a resource person in seminars, symposiums, FDTPS and workshops. He organised many national conferences, seminars, symposiums and workshops for the benefit of faculty and engineering students. Presently, seven PhD scholars are pursuing research under her guidance. His areas of interest are in wireless communication and computer networks.

1 Introduction

Tomography is a non-invasive imaging technique allowing for the visualisation of the internal structures of an object without the superposition of over- and under-lying structures that usually plagues conventional projection images. For example, in a conventional chest radiograph, the heart, lungs and ribs are all superimposed on the same film whereas a computed tomography (CT) slice captures each organ in its actual three-dimensional position. Tomography has found widespread application in many scientific fields including physics, chemistry, astronomy, geophysics and of course, medicine.

The reconstruction of images can be defined as the general problem of estimating a two dimensional object from a degraded version of this object. In image reconstruction, observations result from the interaction between the unknown object and some scattering wave. In fields of tomography, lots of problems are faced in recovering original images from incomplete, indirect and noisy images. Images get corrupted during acquisition by camera sensors, receivers, environmental conditions, improper lightning, undesirable view angle, etc. Also the problem of recovering an original image from noisy image has received an ever increasing attention in recent years.

In computer tomography, an idea of region of interest (ROI) is proposed for image reconstruction where the overall radiation exposure is reduced. It helps to reconstruct a specified region rather than the whole object is required (Sen et al., 2012). They have discussed that projection reconstruction used in MRI being commonly used by other medical imaging techniques like CT or PET was very simple and fast technique for image reconstruction. Fourier-based image reconstruction claiming high reconstruction time, even though parallel-processing techniques are approached (Tugui, 2012). Direct inversion formulae for the two-dimensional (2D) radon transform that are not equivalent to radon's original inversion formula was discussed (Clackdoyle and Noo, 2004). They have discussed about medical imaging. They have also discussed that, with the growth of computers and image technology to diagnosis of a health problem (Ganguly et al., 2010).

At each iteration, the missing views are estimated based on reprojection which is a software substitute for the scanning process (Nassi, 1982). The ROI image reconstruction, the overall radiation exposure is reduced and the problem of tomographic

reconstruction is ill posed. Beside this class of analytic methods, several algebraic methods for the reconstruction from incomplete data were also proposed (Azencott et al., 2007). They have discussed that image reconstruction from projections is the field that lays the foundations for CT (Clackdoyle and Defrise, 2010). They proposed an idea of accurate image reconstruction from highly sparse data in diffraction tomography (Sidky et al., 2009).

The performance of Katsevich reconstruction algorithm proposed which represents a breakthrough for helical cone-beam CT reconstruction (Yan et al., 2011). They discussed on compressed sensing theory which proves that if an object under reconstruction is essentially piecewise constant, a local ROI can be exactly and stably reconstructed via the total variation minimisation (Yu and Wang, 2009).

The iterative ML reconstruction is applied to a ROI without losing the advantages of a ML reconstruction was discussed (Ziegler et al., 2008). They proposed on exact image reconstruction within ROIs from reduced-scan data containing truncations (Zou et al., 2005). They proposed an idea on iterative reconstruction-reprojection (IRR) algorithm for limited projection data CT image reconstruction.

The paper is divided as follows. Section 2 presents the types of image reconstruction such as analytical and iterative reconstructions. Section 3 proposes results of the head photon image using simultaneous algebraic reconstruction technique (SART) algorithm was proposed. Finally, Section 4 concludes with the improvements of the proposed image reconstruction algorithm over the existing random reconstructed image.

2 Types of image reconstruction

Image reconstruction in CT is a mathematical process that generates images from X-ray projection data acquired at many different angles around the patient. Image reconstruction has a fundamental impact on image quality and therefore on radiation dose. Image reconstruction is the creation of two or three dimensional image from scattered or incomplete data such as the radiation readings acquired during a medical imaging study. Different types of reconstruction technique exist. Analytical reconstruction, iterative reconstruction and Fourier reconstruction are some of the reconstruction types.

Methods based on back projection (BP) are one type of analytical reconstruction that is currently widely used on clinical CT scanners because of their computational efficiency and numerical stability. BP is an analytical method which consists of reconstruction kernel. The reconstruction kernel also referred to as ‘filter’ or ‘algorithm’ by some CT vendors, is one of the most important parameters that affect the image quality. There is a tradeoff between spatial resolution and noise for each kernel. A smooth kernel generates images with lower noise but with reduced spatial resolution. A sharp kernel generates images with higher spatial resolution, but increases the image noise. The selection of reconstruction kernel should be based on specific clinical applications.

Iterative reconstruction has recently received much attention in CT because it has many advantages compared with conventional BP techniques. Important physical factors including focal spot and detector geometry, photon statistics, X-ray beam spectrum and scattering can be more accurately incorporated into iterative reconstruction yielding

lower image noise and higher spatial resolution compared with BP. In addition, iterative reconstruction can reduce image artefacts such as beam hardening, windmill and metal artefacts.

Iterative reconstruction refers to iterative algorithms used to reconstruct 2D and 3D images in certain imaging techniques. For example, in CT an image must be reconstructed from projections of an object. Here iterative reconstruction techniques are a better, but computationally more expensive alternative to the common BP method which directly calculates the image in a single reconstruction step.

There are typically five components to iterative image reconstruction algorithms:

- 1 An object model that expresses the unknown continuous-space function that is to be reconstructed in terms of a finite series with unknown coefficients that must be estimated from the data.
- 2 A system model that relates the unknown object to the ‘ideal’ measurements that would be recorded in the absence of measurement noise. Often this is a linear model of the form.
- 3 A statistical model that describes how the noisy measurements vary around their ideal values. Often Gaussian noise or Poisson statistics are assumed.
- 4 A cost function that is to be minimised to estimate the image coefficient vector. Often this cost function includes some form of regularisation. Sometimes the regularisation is based on Markov random fields.
- 5 An algorithm, usually iterative, for minimising the cost function, including some initial estimate of the image and some stopping criterion for terminating the iterations.

The example of such iteration algorithm is algebraic reconstruction techniques (ARTs), simultaneous ART, simultaneous iteration reconstruction techniques, etc.

All iterative reconstruction methods consist of three major steps which are repeated iteratively as visualised in Figure 1. First, a forward projection of the volumetric object estimate creates artificial raw data which, in a second steps are compared to the real measured raw data in order to compute a correction term. In the last step, the correction term is back projected onto the volumetric object estimate.

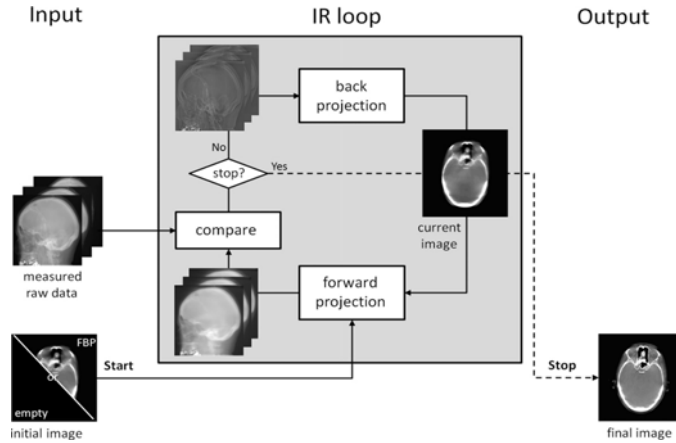
The iteration process can be initiated with an empty image estimate or using prior information, for example, a standard FBP reconstruction or a volume of a similar object. In general, the better the prior images match the final images, the faster the process converges towards a stable solution.

The iterative process is finished when either a fixed number of iterations are reached, or the update for the current image estimate is considered small enough or when a predefined quality criterion in the image estimate is fulfilled. Unfortunately, a general rule of thumb for a termination criterion which exits early enough to avoid unnecessary computations and still guarantees. A satisfactory image quality is hard to give and often depends on the properties of the reconstructed dataset.

The simplest form of iterative reconstruction is the ART, which was already used for the reconstruction of images in the first CT systems ART is based on Kaczmarz’ method for solving linear systems of equations $AXZb$ where in terms of image reconstruction x are the voxels of the volume to be reconstructed, ‘A’ is the system matrix used for producing the raw data and ‘b’ are the pixels of the measured raw data. The entries of the

matrix ‘A’ correspond to rays from the X-ray source through the volume to the detector pixels, i.e., the line integral of the linear attenuation coefficient.

Figure 1 Schematic view of iteration reconstruction process



Often a positivity constraint is applied to the voxels based on the assumption that negative attenuation values are not possible. While the original ART algorithm works on single rays and thus single pixels, the SART performs updates for complete raw data projections.

This leads to a much faster convergence of volumetric images towards a stable solution, but a relaxation factor becomes necessary to keep the noise low and to reduce problems with streak artefacts.

We model a linear imaging system as follows:

$$Ax = b \quad (1)$$

where $A = (A_{i,j})$ denotes an $M \times N$ matrix, $b = (b_1, \dots, b_M)^{tr} \in R^M$ the observed data, $x = (x_1, \dots, x_N)^{tr} \in R^M$ an underlying image.

We use tr for the transpose of a vector/matrix. We define

$$A_{i,+} = \sum_{j=1}^N A_{i,j} \quad \text{for } i = 1, \dots, M, \quad (2)$$

$$A_{+,j} = \sum_{i=1}^M A_{i,j} \quad \text{for } j = 1, \dots, N, \quad (3)$$

$$\tilde{b}(x) = Ax \quad (4)$$

The SART formula is expressed as

$$x_j^{(k+1)} = x_j^{(k)} + \frac{1}{A_{+,j}} \sum_{i=1}^M \frac{A_{i,j}}{A_{i,+}} (b_i - \tilde{b}_i(x^{(k)})) \quad (5)$$

for $k = 0, 1, \dots$. A generalised version was proposed in the above equation

$$x_j^{(k+1)} = x_j^{(k)} + \frac{\omega}{A_{+,j}} \sum_{i=1}^M \frac{A_{i,j}}{A_{i,+}} (b_i - \tilde{b}_i(x^{(k)})) \quad (6)$$

for $k = 0, 1, \dots$, where w denotes a relaxation parameter in $(0, 2)$.

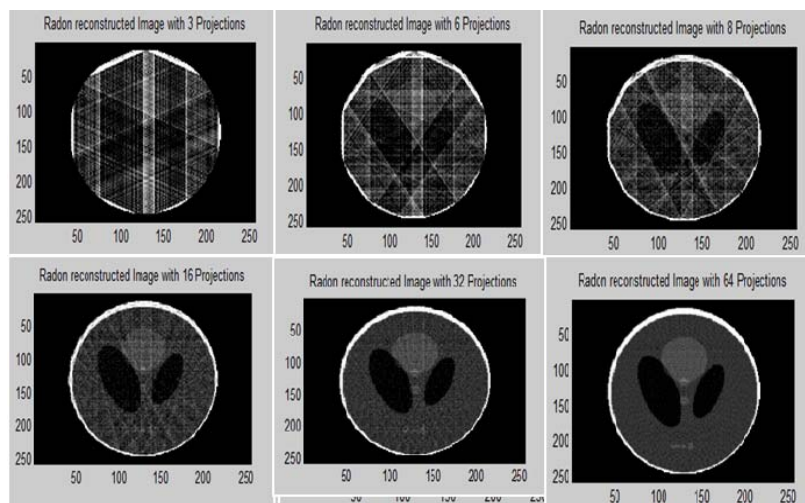
3 Simulation results

As a large number of iteration algorithm are available, it is difficult to select an optimal method for a specific application. The issue here with an example that shows the differences in images of different iteration and projections in random and SART iteration algorithm. A MATLAB generated head phantom image is taken as input shown in Figure 2. The images are obtained by applying the different projection such as 3, 6, 8, 16, 32 using random and SART as shown in Figures 3 and 4. Radon transform which computes projection of an image along specified directions is applied over the head phantom image. By using radon transform slices of different projections is taken. Radon transform is used in the reconstruction of images acquired using projection techniques, specifically X-ray CT scans. The image obtained from radon transform appears blurred. In order to improve the image quality, SART algorithm. The size of the input image is 256×256 .

Figure 2 Head phantom

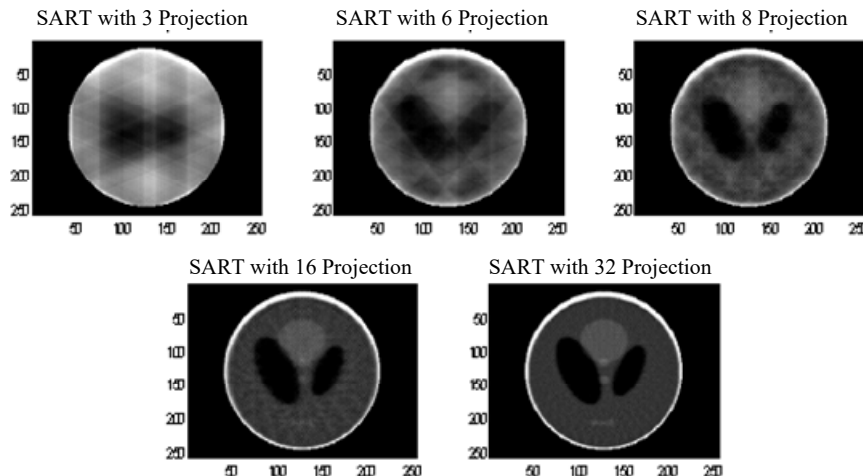


Figure 3 Radon reconstructed image



By increasing the number of projection, the image quality gets improved. Although the quality gets improved, radon reconstructed image appears blurred.

Figure 4 SART reconstructed image



SART is one that updates the value of each pixel one projection at a time. Each pixel of the object to be reconstructed is assigned an initial value. A forward projection is performed and each pixel's value is proportional to the weighted difference between calculated and measured values of all pixels to which that particular pixel contributes.

SART algorithm solves system of consistent linear equations. Smooth images can be obtained when relaxation parameter is introduced. Relaxation parameter is used for fast convergence. If this parameter is carefully adjusted to the reconstruction procedure it can produce efficiently high quality images. Relaxation parameter is denoted as λ . Large values of λ in the interval $(0, 2)$ may lead to fast convergence of SART, but also noisy reconstruction images.

Similarly smaller values of λ lead to smoother images but slower convergence. So λ need to be chosen to ensure fast convergence and good image quality. By selecting the optimal value of λ , with which resolution limit is reached using fewest number of iterations.

In order to reduce the patient exposure to radiation in CT, small number of projections have been explored, e.g., projections restricted to a small ROI. With small set of projections, the tomographic image is reconstructed.

Figures 5 and 6 show that the effect of image quality in terms of mean absolute error (MAE) between original and SART and radon. The image quality can be obtained simply by selection of the number of projection.

The number of projection increases proportionally the difference between the original image and reconstructed image is minimised. However the correlation coefficients are much deviated from original and reconstructed image. To evaluate the effect of thresholding on image quality, they calculated for each type of coefficient selection, the average image error per pixel:

$$\text{average} = \frac{\sum_{x,y} |f(x,y) - h(x,y)|}{MN} \quad (7)$$

where f and h are the reference and reconstructed images respectively with dimensions $M \times N$. Figure 7 shows the correlation coefficient between original and SART Reconstructed image.

Figure 5 MAE between original and radon (see online version for colours)

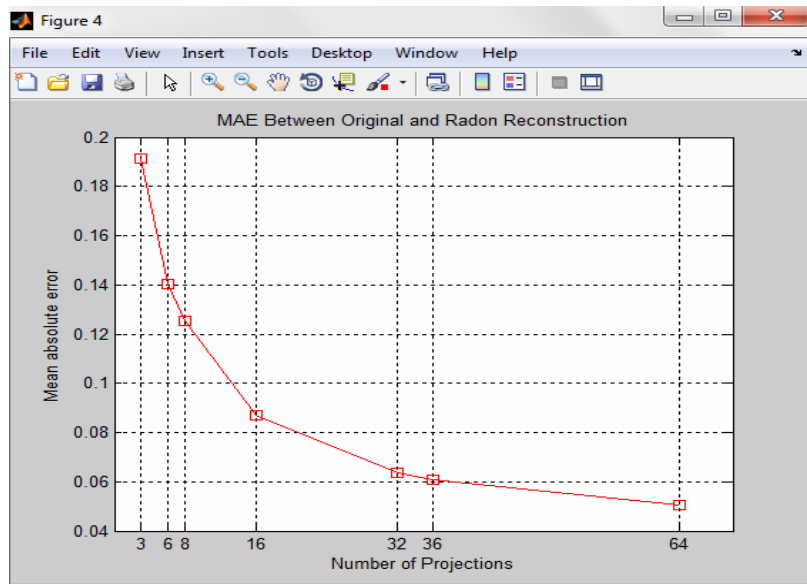


Figure 6 MAE between original and SART (see online version for colours)

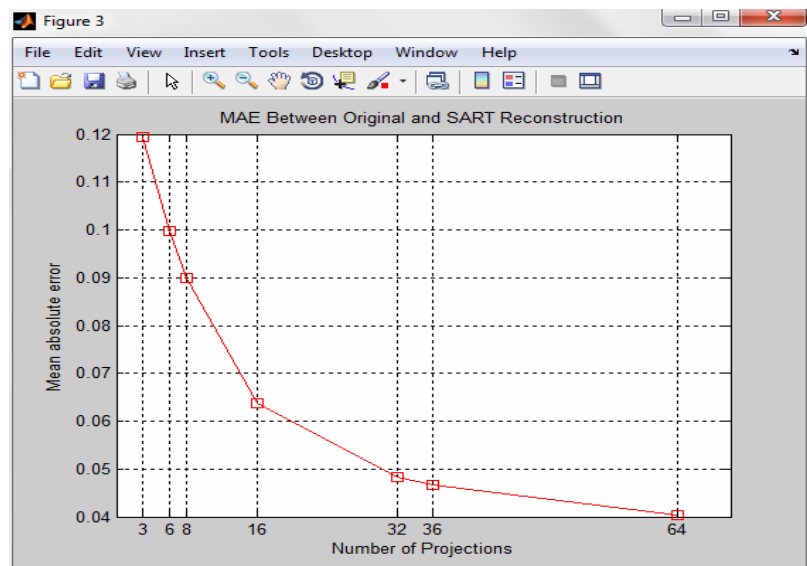
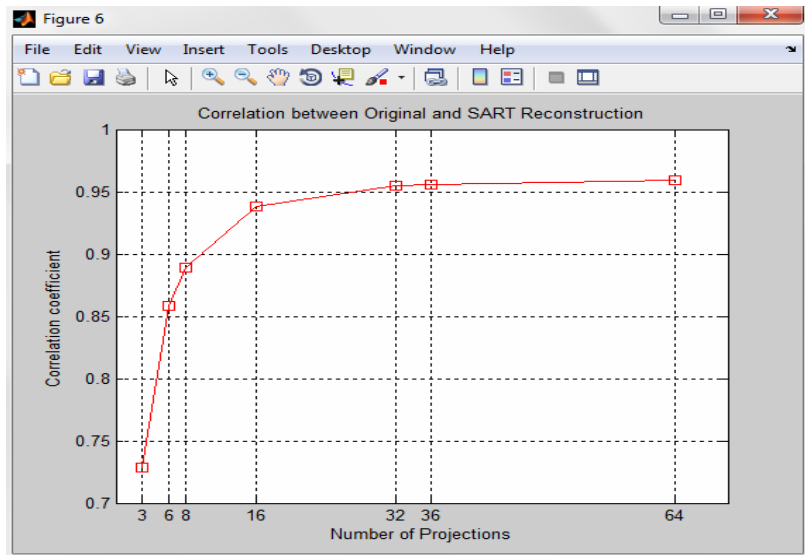


Figure 7 Correlation coefficient between original and SART (see online version for colours)

The MAE and correlation coefficient of the head phantom image is given in Table 1.

Table 1 Mean absolute error

Number of projections	Original image and SART	Original and radon
3	0.1195	0.1912
6	0.0999	0.1405
8	0.0899	0.1254
16	0.0638	0.0868
32	0.0484	0.0638
36	0.0466	0.0610
64	0.0403	0.0507

The MAE of radon reconstructed image and SART reconstructed image is shown above. The SART algorithm provides better results when compared to radon.

Table 2 Correlation co-efficient

Number of projections	Original image and SART	Original and radon
3	0.7289	0.6260
6	0.8580	0.7688
8	0.8890	0.8094
16	0.9385	0.8801
32	0.9547	0.9036
36	0.9560	0.9053
64	0.9593	0.9111

4 Conclusions

The image reconstruction is one of the important issues to be addressed in developing the tomography. In this paper, the performance of iteration based image reconstruction processes along with different projection and image quality are presented. For lower level of iteration number and projections quality of image was less and higher iteration the quality of image was better, but the computation time is much higher. Also the more number of projections, simultaneously improve the quality of image with lower iteration.

References

- Azencott, R., Bodmann, B.G., Labate, D., Sen, A., Patrikeev, I. and Motamed, M. (2007) ‘3D-image reconstruction in highly collimated 3D tomography’, *IEEE Transactions on Biomedical Engineering*, Vol. 2, No. 3, pp.1–9.
- Clackdoyle, R. and Defrise, M. (2010) ‘Tomographic reconstruction in the 21st century’, *IEEE Signal Processing Magazine*, Vol. 27, No. 4, pp.60–80.
- Clackdoyle, R. and Noo, F. (2004) ‘A large class of inversion formulae for the 2-d radon transform of functions of compact support’, IOP publishing *Journal Inverse Problems*, Vol. 20, pp.1281–1291.
- Ganguly, D., Chakraborty, S. and Kim, T-h. (2010) ‘A cognitive study on medical imaging’, *International Journal of Bio-Science and Bio-Technology*, Vol. 2, No. 3, pp.1–18.
- Nassi, M., Brody, W.R., Medoff, B.P. and Macovski, A. (1982) ‘Iterative reconstruction-reprojection: an algorithm for limited data cardiac computed tomography’, *IEEE Transactions on Biomedical Engineering*, Vol. BME-29, No. 5, pp.333–341.
- Sen, A., Labate, D., Bodman, B.G. and Azencott, R. (2012) ‘3D ROI image reconstruction from truncated computed tomography’, *IEEE Transactions on Medical Imaging*, Vol. 11, No. 9, pp.1–24.
- Sidky, E., Kao, C. and Pan, X. (2009) ‘Accurate image reconstruction from few views and limited angle data in divergent beam CT’, *Medical Physics*, Vol. 1, No. 7, pp.312–331.
- Tugui, A. (2012) ‘FFT parallel implementation for MRI image reconstruction’, *U.P.B. Scientific Bulletin – Series C*, Vol. 74, No. 4, pp.229–243.
- Yan, G., Tian, J., Zhu, S., Qin, C., Dai, Y., Yang, F., Dong, D. and Wu, P. (2011) ‘Fast Katsevich algorithm based on GPU for helical cone-beam computed tomography’, *IEEE Transactions on Information Technology in Biomedicine*, Vol. 14, No. 4, pp.214–218.
- Yu, H. and Wang, G. (2009) ‘Compressed sensing based interior tomography’, IOP publishing *Physics in Medicine and Biology*, Vol. 54, pp.2791–2805.
- Ziegler, A., Nielsen, T. and Grass, M. (2008) ‘Iterative reconstruction of a region of interest for transmission tomography’, *Medical Physics*, Vol. 35, No. 4, pp.1317–1327.
- Zou, Y., Pan, X. and Sidky, E. (2005) ‘Image reconstruction in regions-of-interest from truncated projections in a reduced fan-beam scan’, *Physics in Medicine and Biology*, Vol. 50, pp.13–28.



Contents lists available at ScienceDirect

Computers and Electrical Engineering

journal homepage: www.elsevier.com/locate/compeleceng

Peak-power reduction using improved partial transmit sequence in orthogonal frequency division multiplexing systems [☆]

P. Elavarasan ^{*}, G. Nagarajan

Department of ECE, Pondicherry Engineering College, Puducherry 605 014, India

ARTICLE INFO

Article history:

Received 15 May 2014

Received in revised form 14 January 2015

Accepted 14 January 2015

Available online xxxx

Keywords:

OFDM

PAPR

PTS

Phase weighting factor

All Pass Filtering technique

ABSTRACT

Orthogonal Frequency Division Multiplexing (OFDM) system has lead to significant advancement in wireless communication systems. In OFDM system multi-carriers are present. During modulation the sub-carriers are added together with same phase which increases the value of Peak-to-Average Power Ratio (PAPR). High PAPR leads to more interference and reduced resolution of analog to digital converter (A/D) and digital to analog converter (D/A). The Partial Transmit Sequence (PTS) is a popular technique used for PAPR reduction in OFDM systems. The modified PTS technique proposed in this paper overcomes the drawbacks of Original PTS (O-PTS) by making use of Group Phase Weighting Factor (GPW) and Recursive Phase Weighting Factor (RPW) along with All Pass Filtering. Simulations show that the proposed scheme performs very well in terms of PAPR and achieves almost the same Bit Error Rate (BER) performance under Rayleigh fading channel.

© 2015 Elsevier Ltd. All rights reserved.

1. Introduction

Orthogonal Frequency Division Multiplexing (OFDM) is one of the Multi-Carrier Modulation (MCM) techniques that transmit signals by exploiting the advantages of transmission through multiple carriers. OFDM technology has already paved its way into wired and wireless technologies such as the Asymmetric Digital Subscriber Line (ADSL) and the IEEE 802.11 standard [1]. In OFDM, each sub-carrier can be overlapped with the neighborhood sub-carriers. The major advantage of OFDM is that it is robust in a frequency selective fading channel which is a consequence of multipath environment and other communication interferences. The overhead in the technology increases when there is a requirement for large number of sub-carriers. However, requirement of more sub-carriers increases complexity of the modulation, synchronization and coherent demodulation adding to higher hardware cost.

The high Peak-to-Average Power Ratio (PAPR) in OFDM Systems emerges as a big hurdle while migrating to this new technology. The input data stream of the Inverse Fast Fourier Transform (IFFT) should possess a uniform power spectrum, but the output of the IFFT may result in a non-uniform or spiky power spectrum. Most of the transmission energy is sparsely distributed over a few sub-carriers instead of the majority sub-carriers. This problem can be quantified as the PAPR measure.

Jiang and Wu, gave a brief introduction about PAPR reduction techniques in OFDM system for wireless communication and its peak power effects in orthogonal multicarrier modulation [1]. Jayalath and Tellambura discussed about PAPR

[☆] Reviews processed and recommended for publication to the Editor-in-Chief by Associate Editor Dr. Srinivasan Rajavelu.

* Corresponding author.

E-mail addresses: elavarasan_2000@yahoo.co.in (P. Elavarasan), nagarajanpec@pec.edu (G. Nagarajan).

problems in the OFDM system and different reduction techniques in reducing PAPR for OFDM signal [2]. Baxley and Zhou have compared the SLM and PTS techniques for PAR reduction to obtain the desirable PAPR and good system throughput [3]. Lu et al., proposed the technique for PAPR reduction in OFDM based on transformation of partial transmit sequences which give a better performance by trading it, with that of the system complexity [4].

The high PAPR in OFDM signals will reduce the resolution of the Digital-to-Analog (D/A) and Analog-to-Digital (A/D) converters, in both transmitting and receiving ends leading to reduce the efficiency of the amplifier [2–6]. Many methods have been proposed to reduce the PAPR. The literature presents distinct techniques defined in the frequency and time domains. Methods such as Block Coding, Interleaving, Selected Mapping (SLM), Partial Transmit Sequences (PTS), Phase Optimization, Tone reservation and Injection, Precoding, Active Constellation Extension (ACE), Envelope clipping, Companding and Superimposed technique were used to reduce high PAPR [1–8].

The problem of high PAPR is encountered by many reduction techniques and among them Partial Transmit Sequence (PTS) proves to outperform the other methods [5].

This paper mainly focuses on PTS with two phase weighting factors called GPW and RPW along with All Pass Filtering technique to reduce the high PAPR [9–11]. The technique is flexible to control PAPR without destroying the orthogonal property between the sub-carriers. The use of a proper PTS for reducing the PAPR of OFDM signals had been presented in literature [12,13]. In general, the reduction in PAPR can be achieved by the PTS with optimum phase value.

The main drawback of the PTS is its high complexity put together with the problem of finding optimum phase value. The pseudorandom partition PTS is employed making use of the combination of GPW and RPW along with All Pass Filtering technique for the sake of shifting the sub-block sequences to generate new candidates. The proposed scheme can reduce the computational complexity and optimum phase search. Here in the paper, GPW and RPW combined with All Pass Filtering technique and PTS finds optimum phase value in order to reduce the complexity of optimum phase search.

The proposed scheme is advantageous in two aspects: First, with the advent of pseudorandom partition method, reduction in computational complexity is achieved through the dual techniques of GPW and RPW. Second, by utilizing All Pass Filtering technique, the proposed scheme will maintain both the magnitude response and phase shift and it will also eliminate the need of multiple IFFT.

This paper is organized as follows: In Section 2, the system model is introduced and the PTS technique for reducing the PAPR is briefly described. Section 3 gives the necessary conditions on the chosen GPW and RPW along with All Pass Filtering for minimizing the error probability. Section 4 discusses the results from numerical simulations. Finally, Section 5 concludes the paper.

2. PAPR reduction in OFDM

In an OFDM system, a high-rate data stream is split into N low-rate data streams transmitted simultaneously by subcarriers. Each of the sub-carriers is independently modulated and multiplexed. Then, an OFDM signal is obtained by adding up all the independently modulated sub-carriers. The IFFT generates the ready-to-transmit OFDM signal. The sub-carriers are chosen to be orthogonal so that the adjacent sub-carriers can be separated. For an input OFDM block $\mathbf{X} = [X_0 \dots X_{N-1}]^T$, where N is the number of sub-carriers, the discrete-time baseband OFDM signal $x(k)$ can therefore be expressed as

$$x(k) = \frac{1}{\sqrt{N}} \sum_{n=0}^{N-1} X_n e^{\frac{j2\pi k}{N}}, \quad k = 0, 1, \dots, LN - 1 \quad (1)$$

where L is the oversampling factor. It was shown in [11] that the oversampling factor $L = 4$ is sufficient to provide an accurate estimate value of the PAPR of OFDM signals. The PAPR of (k) is defined as the ratio of the maximum instantaneous power to the average power; that is

$$\text{PAPR} = 10 \log_{10} \frac{\max[|X_n|^2]}{E[|X_n|^2]} \quad (2)$$

The PAPR of OFDM signal is defined as the power of a sine wave with amplitude equal to the maximum envelope value which can be computed in the frequency domain because IFFT is a unitary transformation.

The transmitted time signal is usually generated by sampling the continuous time signal. The sampling at Nyquist rate might have a hopeful PAPR value. Hence, for higher value of oversampling factor better PAPR can be achieved. The oversampling factor can be realized by inserting zeros in the middle of the frequency-domain signal and passing the new-point data sequence through the IFFT unit. Therefore, the oversampled IFFT output can be expressed as

$$\hat{x} = \text{IFFT}(\hat{X}) = \sum_{v=1}^V b_v \text{IFFT}(X_v) = \sum_{v=1}^V b_v \cdot X_v \quad (3)$$

In a typical OFDM system with PTS approach to reduce the PAPR, the input data block is divided by means of a pseudo partitioning scheme into disjoint sub-blocks which are represented by the vectors. All the sub-carrier which is present in another block must be zero so that the sum of all the sub-blocks constitutes the original signal. Then, the sub-blocks are transformed into time-domain partial transmit sequence. These partial sequences are independently rotated by the phase

factors and combined together to create a set of candidates. Therefore, total candidates could be generated in O-PTS scheme. Finally, the candidate with the lowest PAPR is chosen by an exhaustive search of the candidates for transmission. In the O-PTS scheme, bits of side information have to be communicated explicitly to the receiver in order to recover the original symbol.

3. Proposed technique

In order to reduce the computational complexity of finding an optimum phase value by the conventional PTS technique, a new technique GPW and RPW along with All Pass Filtering is proposed. The technique offers an enhanced performance in the PAPR reduction compared with that of the existing technique. In proposed technique, all the sub-blocks are split into several disjoint groups and each group can obtain its own subcandidate sequence by using the same set of phase weighting factors as shown in Fig. 1. Then, the subcandidate sequence from different groups are combined together to generate the OFDM candidate sequences. Hence forth the generated candidate sequence that has the least PAPR [9].

3.1. Group Phase Weighting (GPW)

The OFDM sequence can be given by

$$x' = \sum_{i=1}^v b_i x_i + \sum_{i=1}^{v_1} b_i x_i + \sum_{i=r+1}^{v_2} b_i x_i + \cdots + \sum_{i=v_{R-1}+1}^v b_i x_i \quad 1 < r_1 < r_2 < \cdots < r_{R-1} < v$$
 (4)

where the value of r_i , $i = 1, 2, \dots, R-1$, is the index of sub-block. It can be viewed that all the sub-blocks can be split into several groups and for each group the phase weighting can be self implemented. When the number of groups is obtained the subcandidate sequence from the k th group along with the number of sub-blocks in each group can be expressed by $r_1, r_2 - r_1, r_3 - r_2$, where r_1 must be greater than one. By using the same set of phase weighting factors, these groups can be implemented with their respective phase weighting processes which helps to obtain the respective subcandidate sequences. Then, the subcandidate sequences from dissimilar groups can be combined together by complex additions to achieve the OFDM candidate sequences and the one with the least PAPR is selected for transmitting. When the number of sub blocks is 4 ($V = 4$) with a set of phase weighting factors given as $\{1, -1\}$ (i.e., $W = 2$) two sub-blocks in the first group are generated. The four sub-blocks can be split into two groups: one includes the first two sub-blocks and the other contains the remaining sub-blocks. After employing the phase weighting sequences, it is observed that PTS with GPW and O-PTS have the same OFDM candidate sequences.

The performance of proposed PAPR reduction technique is the same as that of O-PTS. As far as computational difficulty is concerned, the complex multiplication is desired by each element in the phase weighting sequence. By which each phase weighting sequence requires the least computational complexity for generating new candidate sequence. Implementation of the proposed technique shows a reduction in computational complexity which is evident from the simulation results. The proposed method can also be modified by using All Pass Filters along with RPW favouring the generation of the optimum phase sequence.

3.2. Recursive Phase Weighting

By considering all the phase weighting sequences, the relationship between phase weighting sequences can be found if the following conditions are satisfied:

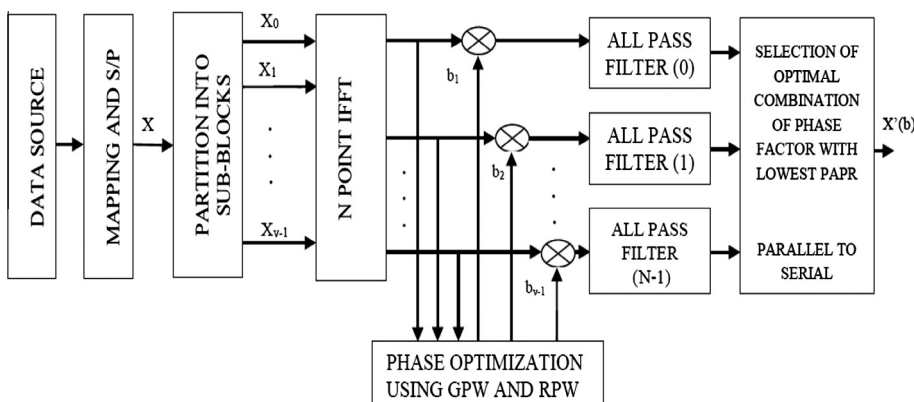


Fig. 1. Block diagram of proposed system model.

- (i) The number of phase weighting factors is even.
- (ii) The set of allowed phase weighting factors is $e^{j(\frac{2\pi k}{W})}$, $[K = 0, 1, \dots, W - 1]$.

The steps involved in the generation and process of phase weighting factors are summarized as follows:

- (i) Phase weighting factors can be generated by using allowable phase weighting sequences.
- (ii) Then the phase weighting sequences can be divided into two equal parts.
- (iii) Different candidate sequences can be obtained by making use of the relationship between two phase weighting sequences. The common terms obtained from the two parts, which are used to compute the candidate sequences. The relationship between two phase weighting sequences from different parts must satisfy the condition that the first phase weighting factors should be same and the remaining part is opposite to each other.
- (iv) By using the common terms mentioned in the above step, different candidate sequences in the other part can be obtained directly by using complex additions.
- (v) By Calculating the PAPR of all the candidate sequences the minimum PAPR is chosen for transmission.

3.3. Combination of GPW and RPW

The two phase weighting methods can be used to reduce the computational complexity and obtain the same PAPR reduction performance as that of the O-PTS. In order to reduce the computational complexity, the combination of GPW and RPW is considered. The PTS considering the effect of combining GPW and RPW is described below:

In the GPW method, all the sub-block sequences are divided into several groups and for each sub-block, the RPW scheme is implemented [10]. During the combination of GPW and RPW the implementation of RPW varies from normal implementation. If the number of sub-blocks in a group is higher than two, the third step in RPW is modified. The sub-blocks can be split into number of small troops. After splitting, each troop should include phase weighting sequences till the last phase weighting factor and the splitting is complete. The opposites of the last phase weighting factors must be in the same troop. After implementing RPW, subcandidate sequences in each group can be obtained. Finally, in terms of GPW, subcandidate sequences from different groups are combined and all the OFDM candidate sequences can be obtained.

3.4. All-Pass Filters

An All-Pass Filter is a signal processing filter that passes all frequencies equally, but changes the phase relationship between various frequencies. It can be done by varying its propagation delay with frequency [11]. An All-Pass Filter passes all input frequencies with the same gain, but it modifies the phase of the signals. All-Pass Filter has a gain of one and such filters are used for group delay equalization, notch filtering design, Hilbert transform implementation and musical instruments synthesis. All Pass-Filters, delay the OFDM sequence by providing delay and reduced interference. In a PTS scheme, different frequency domain OFDM sequences are generated and then transformed into time domain sequences by using multiple IFFT modules. In the proposed scheme, different OFDM sequences are directly generated in the time domain, hence the need for IFFT modules can be eliminated. Generation of the alternative time domain OFDM sequences can be performed using multiple All-Pass Filters. The general function of an All-Pass Filter is given by

$$H(Z) = \prod_{k=1}^K \frac{Z^{-1} - c_k^*}{1 - c_k Z^{-1}} \quad (5)$$

where c_k , c_k^* and K are the k th complex pole, its complex conjugate and the number of the complex poles, respectively. The magnitude response $|H(e^{j\omega})|$ and the phase response are given as angle of $|H(e^{j\omega})|$ are given as

$$|H(e^{j\omega})| = 1 \quad (6)$$

Thus the existing scheme has a drawback of providing lesser number of choices for selecting the optimum phase sequence in O-PTS methods. Therefore the proposed scheme which has a prime advantage that it has more PAPR reduction capability.

4. Simulation results

To illustrate the performance of the proposed scheme, extensive simulations result were carried out to evaluate the performance of PAPR reduction. Error probability and Bit Error Rate (BER) at the receiver were estimated. The simulation parameters are tabulated in Table 1. The results of the simulations are based on the transmission of pseudo randomly generated OFDM symbols with the carriers for Quadrature Phase Shift Keying (QPSK) modulation technique. The Complementary Cumulative Density Function (CCDF) of the PAPR is used to measure the performance at the transmitter side. Cumulative Distribution Function (CDF) of the PAPR is one of the most frequently used performance measures for PAPR reduction techniques. In the literature, CCDF is commonly used instead of the CDF. The CCDF of the PAPR denotes the probability that the

Table 1
Simulation parameters.

Parameters	Details
Software tool	MATLAB 7.9
Sub-carrier	128, 256, 512 and 1024
No. of sub blocks	2, 4, 6 and 8
Modulation	QPSK
Phase set	2 and 4
Channel used	Rayleigh channel

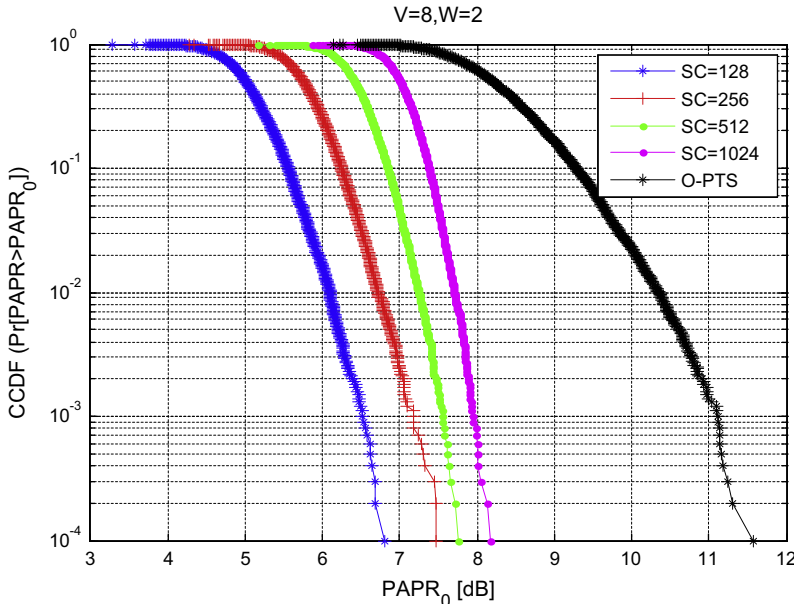


Fig. 2. Comparison of PAPR reduction between proposed scheme and O-PTS under $V = 8$ and $W = 2$.

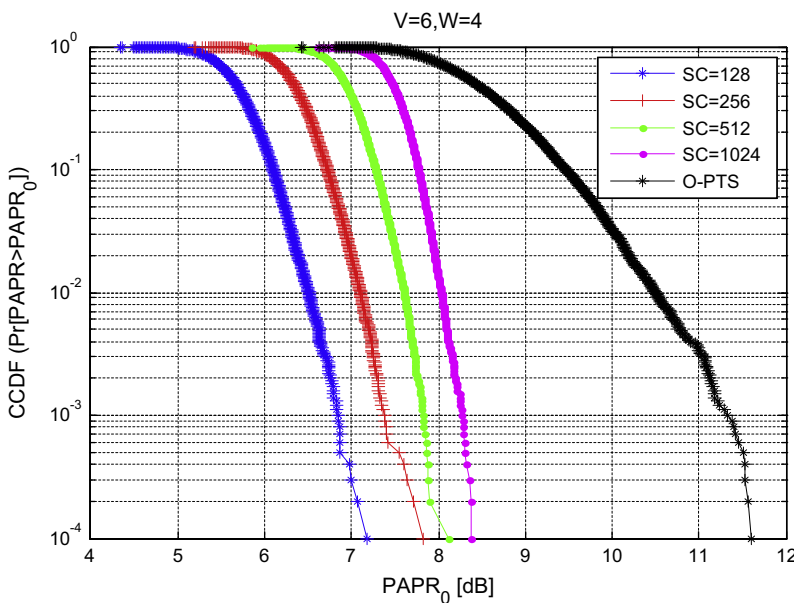


Fig. 3. Comparison of PAPR reduction between proposed scheme and O-PTS under $V = 6$ and $W = 4$.

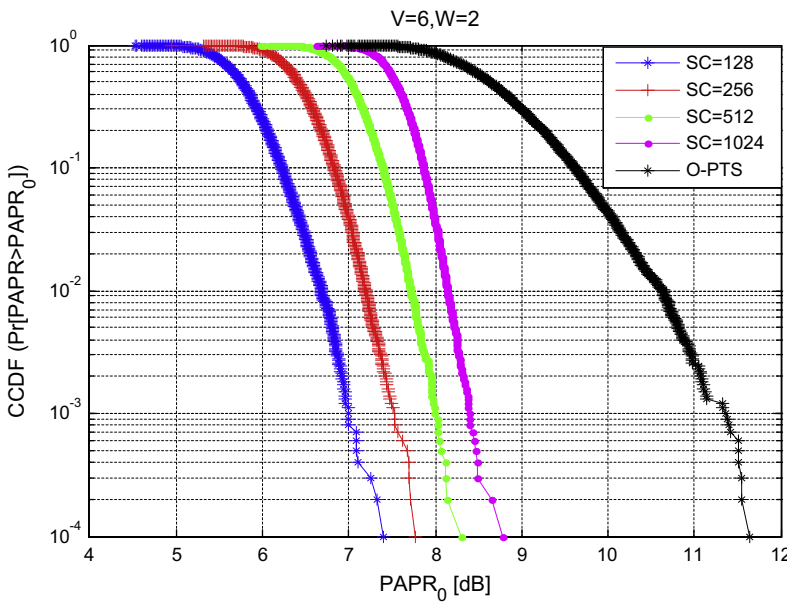


Fig. 4. Comparison of PAPR reduction between proposed scheme and O-PTS under $V = 6$ and $W = 2$.

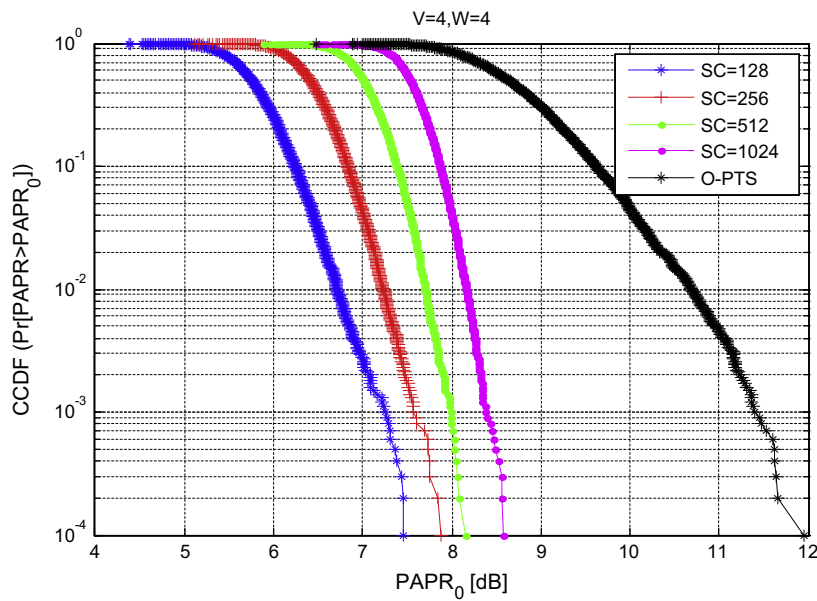


Fig. 5. Comparison of PAPR reduction between proposed scheme and O-PTS under $V = 4$ and $W = 4$.

PAPR of a data block exceeds a given threshold. In [1], a simple approximate expression is derived for the CCDF of the PAPR of a multicarrier signal with Nyquist rate sampling. The CDF of the amplitude of a signal sample is given by

$$F(z) = 1 - \exp(-z) \quad (7)$$

Moreover, the distribution of PAPR bears stochastic characteristics in a practical OFDM system, usually being expressed in terms of CCDF. The CCDF can also be used to evaluate and compare the performance of any PAPR reduction schemes and the CCDF of discrete-time PAPR is given by

$$\text{CCDF}(N, \text{PAPR}_0) = \Pr\{\text{PAPR} > \text{PAPR}_0\} = 1 - (1 - e^{-\text{PAPR}_0})^N \quad (8)$$

where N is the number of sub-carriers in an OFDM system.

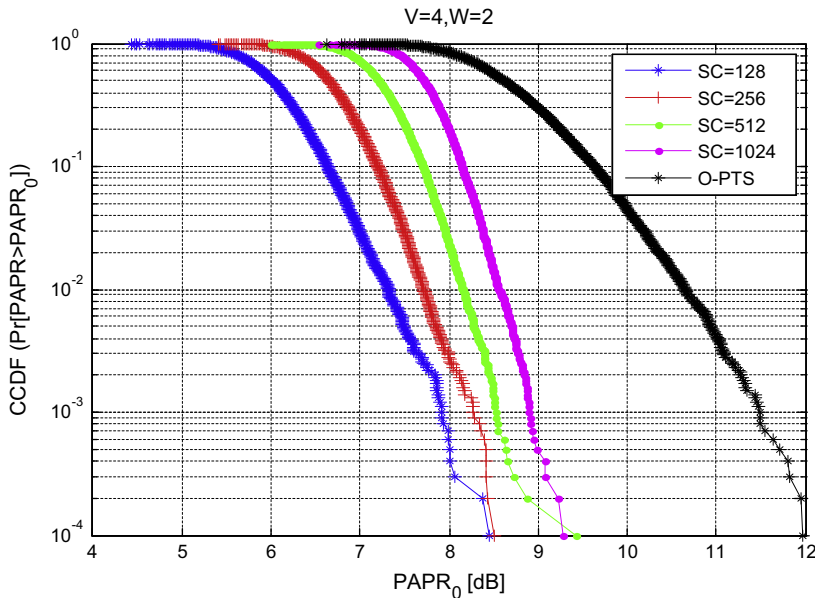


Fig. 6. Comparison of PAPR reduction between proposed scheme and O-PTS under $V = 4$ and $W = 2$.

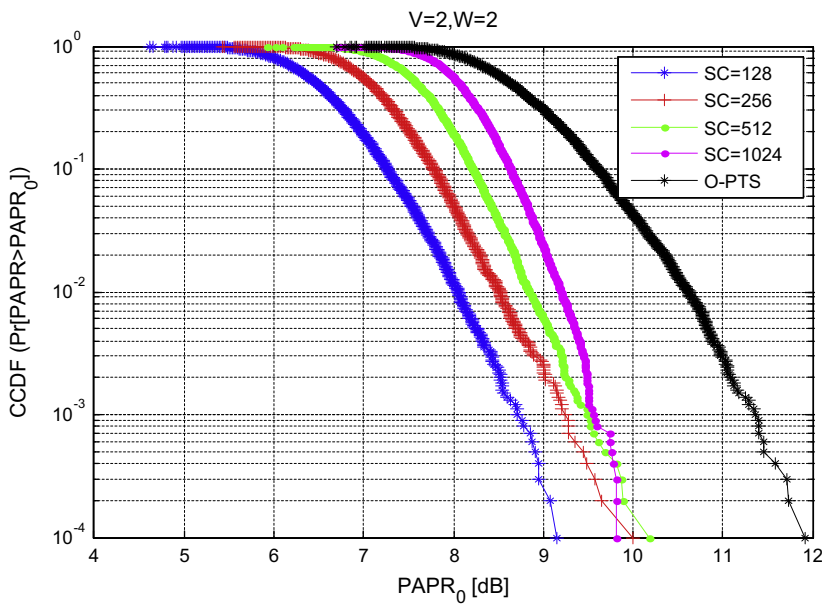


Fig. 7. Comparison of PAPR reduction between proposed scheme and O-PTS under $V = 2$ and $W = 2$.

Therefore, there have been many attempts to derive more accurate distribution of PAPR. The CCDFs of the proposed PTS scheme with sub-block varies from 2 to 8 and phase value is used as 2 and 4. To illustrate the effectiveness of the proposed scheme, several simulations result were used to evaluate the performance in terms of PAPR reduction, estimation of error probability of the detector as well as BER. The results of the simulation are based on the transmission of randomly generated OFDM symbols. By increasing the number of sub-blocks, the proposed system requires low transmitted power.

As far as PAPR reduction performance is concerned, the CCDF is used to evaluate and compare the different PAPR reduction schemes. Figs. from 2 to 7 show the performance comparison between the proposed scheme and existing O-PTS in terms of CCDF. The proposed PTS scheme has the ability to generate more candidates with the same parameters. The PAPR performance can be increased when more number of sub-blocks and phase values are selected. Fig. 2 shows the performance comparison with different sub-carriers for $V = 8$ and $W = 2$. For fairness of comparison of the PAPR performance.

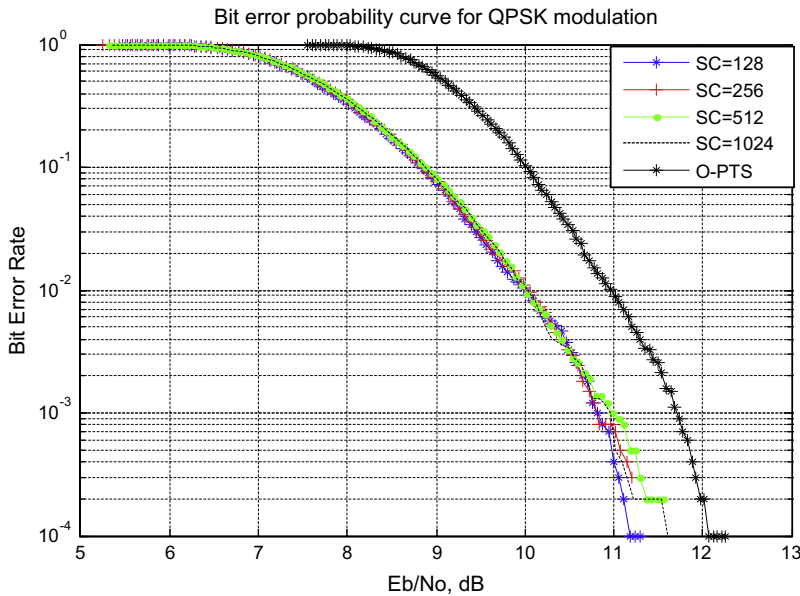


Fig. 8. Comparison of PAPR reduction between proposed scheme for Eb/No Vs BER under $V = 8$ and $W = 2$.

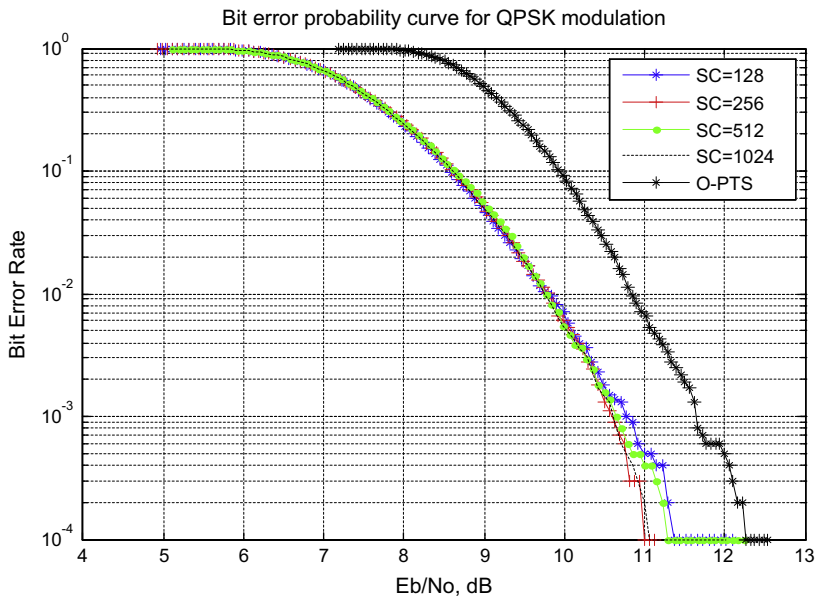


Fig. 9. Comparison of PAPR reduction between proposed scheme for Eb/No Vs BER under $V = 6$ and $W = 4$.

Fig. 3 plots the curves of the proposed PTS scheme with the candidates, which are the same as that of O-PTS scheme. The result shows that the proposed PTS scheme can obtain better PAPR performance. In Fig. 3 the CCDF of the PAPR_0 is simulated for the OFDM system with various sub-carriers and with modulation techniques. This is compared with the O-PTS, as shown in Fig. 4. It can be observed that the PAPR of the proposed method is better by 3 dB at the probability of 10^{-4} .

From Fig. 4, it can be found, that the 3 dB improvement in PAPR_0 depends on the number of sub-blocks and the modulation scheme employed. As number of GPW and RPW factors are increased, the performance of proposed PTS scheme increases for better distinction between shifted and non-shifted symbols after transmission through the channel. Moreover, computational complexity is reduced for the number of fixed sub-blocks in the proposed scheme. When the number of disjoint groups and sub-blocks are increased, more PAPR can be reduced in proposed scheme compared to O-PTS. Increases in

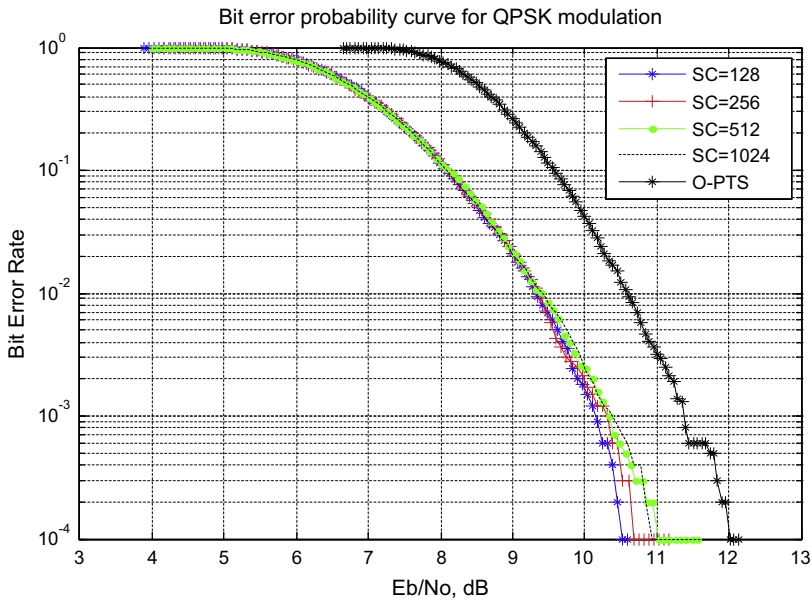


Fig. 10. Comparison of PAPR reduction between proposed scheme for Eb/No Vs BER under $V = 6$ and $W = 2$.

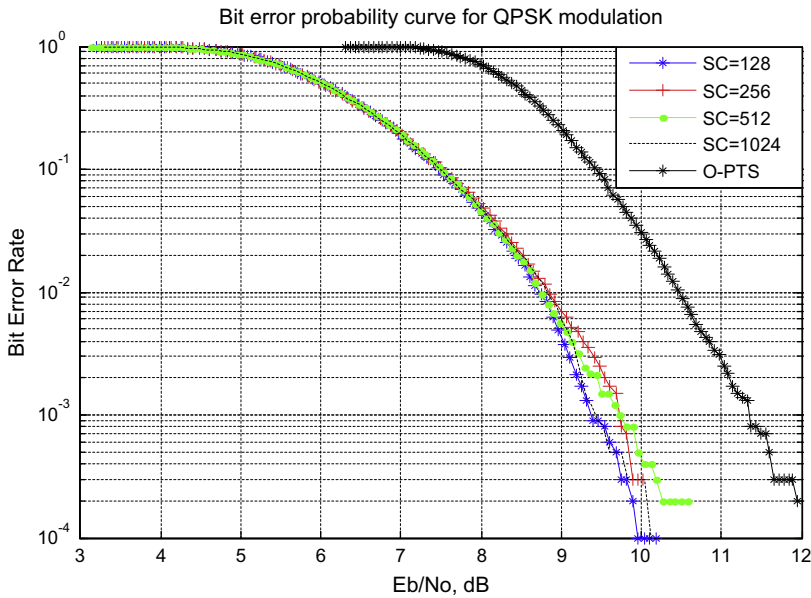


Fig. 11. Comparison of PAPR reduction between proposed scheme for Eb/No Vs BER under $V = 4$ and $W = 4$.

size of each group result in more reduction in computational complexity. The performance improvement of the proposed scheme is around 2.5 dB as shown in Figs. 5 and 6.

When compared to O-PTS scheme, the PAPR performance of the proposed PTS scheme also improves between 1.8 dB and 2.5 dB with the same parameters of $V = 2$, $W = 2$ as shown in Fig. 7. Hence it can be observed that the GPW and RPW along with all pass filter reduces computational complexity. Figs. 8–13 illustrate the probability of detection failure against the Signal Noise Ratio (SNR) of the proposed scheme. Fig. 8 shows the proposed scheme with sub-block variations from 128 to 1024. QPSK modulation method is employed over Rayleigh fading channel. The proposed scheme can be implemented at the receiver's side to improve the performance of OFDM system. It can perform better than O-PTS scheme at the receiver side. Moreover, if GPW and RPW are performed with all pass filter technique, the complexity is further reduced over Rayleigh fading

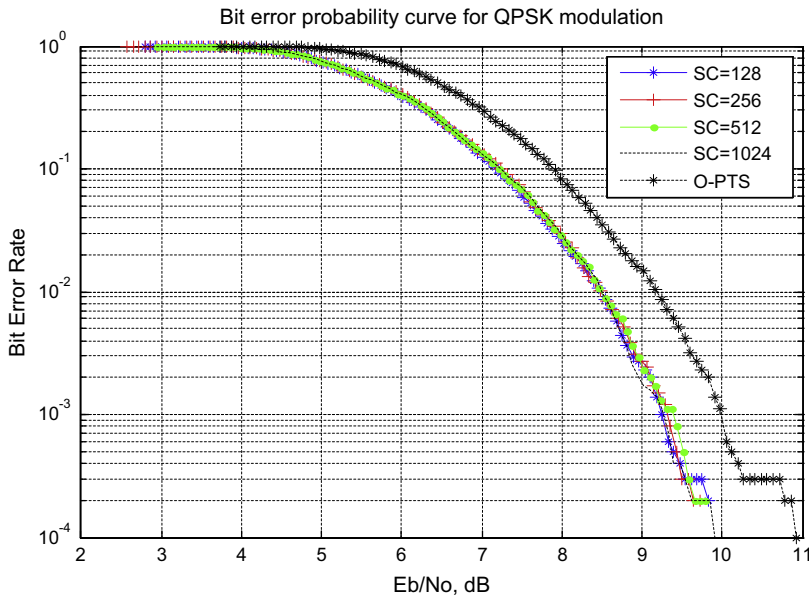


Fig. 12. Comparison of PAPR reduction between proposed scheme for Eb/No Vs BER under $V = 4$ and $W = 2$.

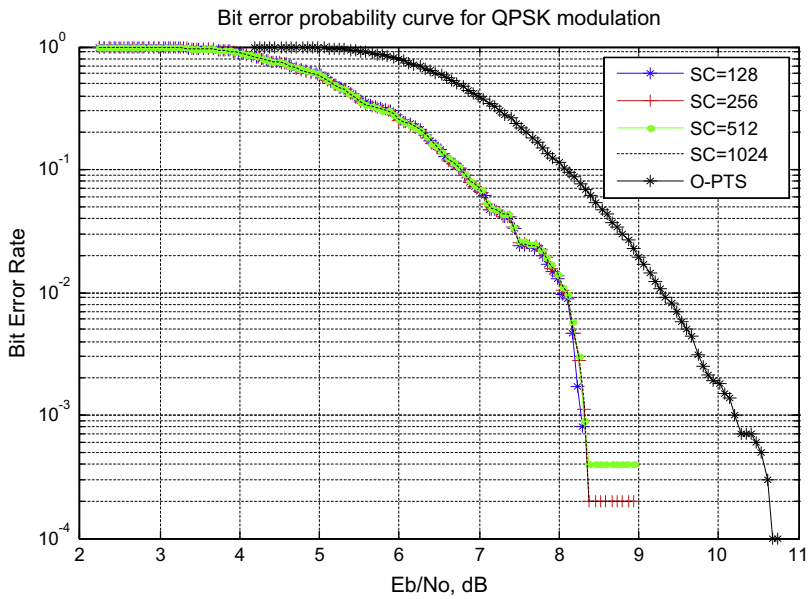


Fig. 13. Comparison of PAPR reduction between proposed scheme for Eb/No Vs BER under $V = 2$ and $W = 2$.

channels. It can be observed that as the number of sub-blocks is increased, the performance of proposed PTS scheme also increases with more number of Rayleigh fading channels.

It can be observed that as the number of sub-blocks is increased, the performance of proposed PTS scheme also increases with more number of phase values.

There may be degradation in the performance of receiver due to the reduction of transmission power. Figs. 8–13 demonstrate the reliability of the detector for the proposed PTS scheme. It is obvious that a good BER performance is maintained in the proposed PTS scheme when compared with O-PTS using optimum 'V' and 'W'. The BER performance of the proposed PTS scheme over Rayleigh fading channel for number of sub-blocks from 2 to 8 employing QPSK is presented. QPSK with Rayleigh fading environment provides a favorable trade-off between the PAPR reduction and the BER. Table 2 gives CCDF and BER of the proposed scheme compared to O-PTS.

Table 2

Performance of proposed scheme.

Transmitter side PAPR ₀ at 10 ⁻⁴							BER at 10 ⁻⁴ (receiver side)				
GPW and RPW	Sub-carriers	O-PTS	1024	512	256	128	O-PTS	1024	512	256	128
V = 2	W = 2	12	10.2	10	9.9	9.2	10.8	8.8	8.7	8.4	8.4
	W = 2	12	8.8	8.3	8.6	8.4	11	9.9	9.7	9.7	9.6
	W = 4	12	8.6	8.2	7.9	7.5	11.8	10.8	10.6	10.2	10
V = 6	W = 2	11.9	8.8	8.3	7.9	7.4	12	11	10.8	10.6	10.5
	W = 4	11.7	8.4	8.2	7.8	7.2	12.2	11.5	11.3	11.1	11
V = 8	W = 2	11.8	8.2	7.8	7.5	7	12.2	11.6	11.4	11.3	11.2

While employing PTS scheme which can be regarded as the phase modification for each sub-carrier signal in the frequency domain, but without incurring any signal distortion, it is found that the spectrum of each sub-carrier signal is still unaffected. Thus, PTS scheme causes no change in the spectrum of original OFDM signals. The proposed scheme making use of GPW and RPW along with all pass filter reduces computational complexity and maintains the same candidate sequences as that of O-PTS. Also it causes no change in the spectrum of original OFDM signals.

5. Conclusion

The proposed method for PAPR reduction in OFDM systems is based on a combination of the GPW and RPW together with All Pass Filtering. Using the Pseudo random partitioning PTS scheme by employing this method, the computational complexity is reduced and also the PAPR performance increases even at a minimum operating power of the amplifier. The proposed scheme reduces the complexity due to following reasons: the GPW and RPW combination generates more number of phase factors and select the optimum one. Secondly, the All Pass Filtering technique maintains the magnitude response and optimum phase shift. Thirdly by combining these two techniques and the need of multiple IFFT is eliminated. Simulation results show that the proposed scheme is more reliable. Also it achieves nearly the same BER performance as achieved by the conventional PTS scheme in a Rayleigh fading environment.

References

- [1] Jiang T, Wu Y. An overview: peak-to-average power ratio reduction techniques for OFDM signals. *IEEE Trans Broadcast* 2008;54(2):257–68.
- [2] Jayalath ADS, Tellambura C. SLM and PTS peak-power reduction of OFDM signals without side information. *IEEE Trans Wireless Commun* 2005;4(5):2006–13.
- [3] Baxley RJ, Zhou GT. Comparing selected mapping and partial transmit sequence for PAR reduction. *IEEE Trans Broadcast* 2007;53(4):797–803.
- [4] Lu G, Wu P, Carleilmalm-Logothetis C. Peak-to-average power ratio reduction in OFDM based on transformation of partial transmit sequences. *Elec Lett* 2006;42(2):105–6.
- [5] Kang SG, Kim JG, Joo EK. A novel sub block partition scheme for partial transmits sequence OFDM. *IEEE Trans Broadcast* 1999;45(3):333–8.
- [6] Armstrong J. Peak-to-average power reduction for OFDM by repeated clipping and frequency domain filtering. *Electron Lett* 2002;38(5):246–7.
- [7] Chen JC. Application of quantum-inspired evolutionary algorithm to reduce PAPR of an OFDM signal using partial transmit sequences technique. *IEEE Trans Broadcast* 2010;56(1):110–3.
- [8] Hao MJ, Lai CH. Precoding for PAPR reduction of OFDM signals with minimum error probability. *IEEE Trans Broadcast* 2010;56(1):120–8.
- [9] Ho WS, Madhukumar AS, Chin F. Peak-to-average power reduction using partial transmit sequences: a suboptimal approach based on dual layered phase sequencing. *IEEE Trans Broadcast* 2003;49(2):225–31.
- [10] Wang Lingyin, Liu Ju. PAPR reduction of OFDM signals by PTS with grouping and recursive phase weighting methods. *IEEE Trans Broadcast* 2011;57(2).
- [11] Hong E, Har D. Peak-to-average power ratio reduction in OFDM systems using all-pass filters. *IEEE Trans Broadcast* 2010;56(1):114–9.
- [12] Hou J, Ge J, Zhai D, Li J. Peak-to-average power ratio reduction of OFDM signals with nonlinear companding scheme. *IEEE Trans Broadcast* 2010;56(2):258–62.
- [13] Jiang T, Guizani M, Chen HH, Xiang W, Wu Y. Derivation of PAPR distribution for OFDM wireless systems based on extreme value theory. *IEEE Trans Wireless Commun* 2008;7(4):1298–305.

P. Elavarasan received his B.E. in Electronics and Communication Engineering from Anna University, Chennai in 2007 and M.Tech in Electronics and Communication Engineering from Pondicherry Engineering College, Puducherry in 2009. He is currently a research scholar with the Pondicherry Engineering College, Puducherry. His research is focused on exploring different PAPR reduction techniques in OFDM systems.

G. Nagarajan completed his B.E. from Madurai Kamaraj University in 1989 and M.Tech in Electronics and Communication Engineering from Pondicherry Engineering College in 1996. He got his Ph.D from Pondicherry University in the field of Wireless Communication in 2007. He is currently Professor in Department of ECE, Pondicherry Engineering College. His area of interest includes OFDM Systems and Mobile Computing.



A Summarization on PAPR Techniques for OFDM Systems

Parthasarathy Elavarasan · G. Nagarajan

Received: 24 November 2012 / Accepted: 31 August 2014
© The Institution of Engineers (India) 2014

Abstract Communication is one of the main aspects of life. With the advancement in age and its growing demands, there has been rapid growth in the field of communications. Signals, which were initially sent in the analog domain, are being sent in the digital domain. For better transmission, still the single carrier waves are being replaced by multi carriers. Multi carrier systems like CDMA and OFDM are now a day being implemented normally. In the OFDM system, orthogonally placed sub carriers are used to carry the data from the transmitter end to the receiver end. Presence of guard band in this system deals with the problem of ISI and noise is minimized by larger number of sub carriers. But the large peak to average power ratio (PAPR) of these signal have some undesirable effects on the system. This paper focuses on presenting the basics of an OFDM system and various methods to reduce the PAPR. High peak to average power ratio of the transmit signal is a major drawback of multicarrier transmission in OFDM. This article describes some of the important PAPR reduction techniques for multicarrier transmission including amplitude clipping and filtering, coding, partial transmit sequence, selected mapping, interleaving, tone reservation, tone injection and active constellation extension. Finally the criterion for PAPR reduction technique selection has been discussed.

Keywords OFDM · PAPR · CCDF · Amplitude clipping and filtering · SLM · PTS

Introduction

Orthogonal frequency division multiplexing (OFDM) is a special form of multicarrier modulation which is particularly suited for transmission over a dispersive channel. Here the different carriers are orthogonal to each other, that is, they are totally independent of one another [1]. This is achieved by placing the carrier exactly at the nulls in the modulation spectra of each other as shown in Fig. 1.

OFDM uses the overlapped orthogonal signals which divide a frequency-selective channel into number nonoverlapped narrowband flat-fading channels. Instead of transmitting the data symbols consecutively at a high symbol rate on a single carrier, a group of symbols is encoded using the fast Fourier transform (FFT) and transmitted in parallel over a number of subchannels. The subchannels are spaced equally by the inverse of the symbol time, making them orthogonal. Individual subchannels will have a longer symbol period than the multipath delay spread and so OFDM is constructively useful for avoiding multipath interference. If a particular subchannel has high noise or interference, then it can be eliminated, reducing the effects of fading and interference. Firstly, the guard bands and cyclic prefix reduce data throughput and system efficiency. Frequency offsets between transmitter and receiver must be removed with automatic frequency control (AFC), otherwise the subcarriers will not be orthogonal. Synchronization of multicarrier schemes is more complex compared to single carrier because there may be hundreds of samples per multicarrier symbol. Due to these advantages of the OFDM system, it is vastly used in various communication systems. Finally, there are a large number of subcarriers, which combined together have a large peak-to-average power ratio (PAPR),

P. Elavarasan (✉) · G. Nagarajan
Department of Electrical Communication Engineering,
Pondicherry Engineering College, Puducherry 605014, India
e-mail: elavarasan_2000@yahoo.co.in

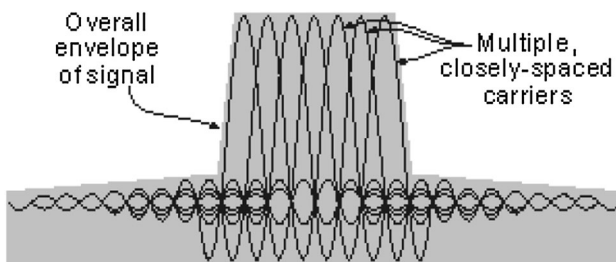


Fig. 1 Frequency spectrum for an OFDM system with N carriers

and to maintain linearity over this range, the power amplifier (PA) requires back-off by as much as 10 dB. OFDM is very attractive for mobile radio transmission where multipath interference is severe.

But the major problem one faces while implementing this system is the high peak to average power ratio. A large PAPR increases the complexity of the analog to digital (A/D) and digital to analog (D/A) converter and reduces the efficiency of the radio frequency (RF) power amplifier [2, 3].

Regulatory and application constraints can be implemented to reduce the peak transmitted power, which in turn reduces the range of multi carrier transmission [4, 5].

This leads to the prevention of spectral growth and the transmitter power amplifier is no longer confined to linear region in which it should operate. This has a harmful effect on the battery lifetime.

Thus in communication system, it is observed that all the potential benefits of multi carrier transmission can be outweighed by a high PAPR value. There are a number of techniques to deal with the problem of PAPR. Some of them are ‘amplitude clipping and filtering’, ‘coding’, ‘partial transmit sequence (PTS)’, ‘selected mapping (SLM)’ and ‘interleaving’. These techniques achieve PAPR reduction at the expense of transmit signal power increase, bit error rate (BER) increase, data rate loss, computational complexity increase, and so on.

Modulation and Demodulation in OFDM Systems

Modulation is the technique by which the signal wave is transformed over the communication channel in order to minimize the effect of noise. In an OFDM system, the high data rate information is divided into small packets of data which are placed orthogonal to each other [4]. This is achieved by modulating the data by a desirable modulation technique. After this, inverse fast fourier transform (IFFT) is performed on the modulated signal, which is further processed bypassing through a parallel to serial converter. In order to avoid Inter symbol interference (ISI) a cyclic prefix to the signal [5] is provided.

Sub Carriers

Each sub carrier in an OFDM system is a sinusoidal signal with a frequency that is an integer multiple of a fundamental frequency. Each sub carrier is like a Fourier series component of the composite signal, in OFDM system [6].

The sum of the sub carriers in the baseband OFDM signal can be given by:

$$\sum a_n \cos \omega_n t + j b_n \sin \omega_n t \quad (1)$$

where, a_n and b_n are the in-phase and quadrature modulating symbols.

Inter Symbol Interference (ISI) and Inter Carrier Interference (ICI)

Inter symbol interference is a form of distortion of a signal in which one symbol interferes with subsequent symbols. Presence of Doppler shifts, frequency and phase offsets in an OFDM system causes loss in orthogonality of the sub carriers. As a result, interference is observed between sub carriers. This phenomenon is known as Inter carrier interference (ICI) [7].

Cyclic Prefix

The cyclic prefix or guard Interval is a periodic extension of the last part of an OFDM symbol that is added to the front of the symbol in the transmitter and is removed at the receiver before demodulation as shown in Fig. 2.

Communication Channel

This is the channel through which the data is transferred. Presence of noise in this medium affects the signal and causes distortion in its data content.

Demodulation

Demodulation is the process by which the original data (or a part of it) is recovered from the modulated signal. In this

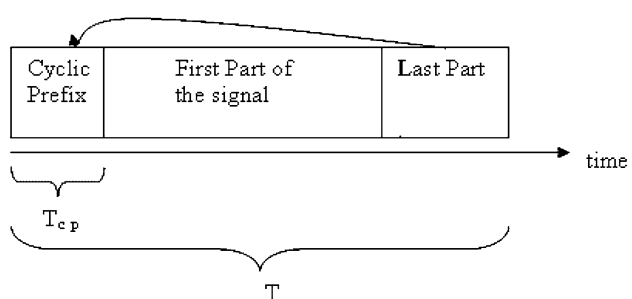


Fig. 2 Cyclic prefix

case, the received data is first made to pass through a low pass filter and the cyclic prefix is removed [8].

OFDM Reception

Two other important parts of the processing of the received OFDM signal are synchronization and channel estimation.

Synchronization

At the front-end of the receiver, OFDM signals are subject to synchronization errors due to oscillator impairments and sample clock differences. The demodulation of the received radio signal to baseband involves oscillators whose frequencies may not be perfectly aligned with the transmitter frequencies. This results in a carrier frequency offset [4]. These errors can occur at the front end of an OFDM receiver. Also, demodulation usually introduces phase noise acting as an unwanted phase modulation of the carrier wave.

Channel Estimation

Channel Estimation in OFDM is usually performed with the aid of pilot symbols. Since each subcarrier is flat fading, techniques from single-carrier flat fading systems are directly applicable to OFDM. For such systems pilot-symbol assisted modulation (PSAM) on flat fading channels involves the sparse insertion of known pilot symbols in a stream of data symbols [8]. The attenuation of the pilot symbols is measured and the attenuations of the data symbols in between these pilot symbols are typically estimated.

Principles of OFDM

OFDM is a block transmission technique. The transmitted OFDM signal multiplexes several low-rate data streams, each data stream is associated with a given subcarrier. The main advantage of this concept in a radio environment is that each of the data streams experiences an almost flat fading channel. In slowly fading channels, the ISI and ICI within an OFDM symbol can be avoided with a small loss of transmission energy, using the concept of a cyclic prefix.

Signal Characteristics

An OFDM signal consists N orthogonal subcarriers modulated by N parallel data streams. Each baseband subcarrier is of the form

$$\varphi_k(t) = e^{j2\pi f_k t} \quad (2)$$

where, f_k is the frequency of the subcarrier. One baseband OFDM symbol (without a cyclic prefix) multiplexes N modulated subcarriers:

$$s(t) = \frac{1}{\sqrt{N}} \sum_{k=0}^{N-1} x_k \varphi_k, \quad 0 < t < N \quad (3)$$

where, x_k is the k^{th} complex data symbol (typically taken from a PSK or QAM symbol constellation) and NT is the length of the OFDM symbol. The subcarrier frequencies f_k are equally spaced which makes the subcarriers orthogonal

$$f_k = \frac{K}{NT} \quad (4)$$

which makes the subcarriers f_k on $0 < t < NT$ orthogonal. The signal separates data symbols in frequency by overlapping subcarriers, thus using the available spectrum in an efficient way. As the OFDM signal is the sum of a large number of independent, identically distributed component its amplitude has an approximately Gaussian distribution by the central limit theorem [1–3]. Therefore, it suffers from large PAPR. Large PAPR also cause out-of-band emission because of amplifier nonlinearity.

PAPR of a Multicarrier Signal

Let, the data block of length N is represented by a vector and duration of any symbol in the set X is T and represented by one of the sub carriers set. As the N sub carriers chosen to transmit the signal are orthogonal to each other and NT is the duration of the OFDM data block X , the PAPR of the transmitted signal is defined as reducing the max (X_n) which is the principle goal of PAPR reduction techniques. Since, discrete-time signals are deal with in most systems, many PAPR techniques are implemented to deal with amplitudes of various samples.

Cumulative Distribution Function

The Cumulative Distribution Function (CDF) is one of the most regularly used parameter which is used to measure the efficiency of any PAPR technique. Normally, the Complementary CDF (CCDF) is used instead of CDF, which helps us to measure the probability that the PAPR of a certain data block exceeds the given threshold [9]. By implementing the Central Limit Theorem for a multi carrier signal with a large number of subcarriers, the real and imaginary part of the time domain signals have a mean of zero and a variance of 0.5.

Peak to Average Power Ratio (PAPR)

Basically PAPR is the most popular parameter used to evaluate the dynamic range of the time-domain OFDM signal or signals envelop variation. In practical systems, a guard interval (cyclic prefix) is inserted by the transmitter in order to remove Inter-Symbol Interference (ISI) and Inter-Channel Interference (ICI) in the multipath environment. However, it can be ignored since it does not affect the PAPR [4]. The PAPR of the transmit signal $s(t)$, defined as the ratio of the maximum instantaneous power and the average power is given by

$$\text{PAPR} = 10 \log_{10} \frac{\max[|X_n|^2]}{E[|X_n|^2]} \quad (5)$$

where, E denotes the expectation operator. Usually, the continuous time PAPR of X_n is approximated using the discrete time PAPR.

Presence of large number of independently modulated sub-carriers in an OFDM system, the peak value of the system can be very high as compared to the average of the whole system. This ratio of the peak to average power value is termed as PAPR.

The major disadvantages of a high PAPR are:

- Increased complexity in the analog to digital and digital to analog converters.
- Reduction in efficiency of RF amplifiers.

Techniques to Reduce the PAPR

An OFDM signal has an approximately Gaussian amplitude distribution when the number of subcarriers is large. Therefore, very high peaks in the transmitted signal can occur. This property is often measured via the signal's peak-to-average power ratio [10]. To be able to transmit and receive these peaks without clipping the signal, the A/D and D/A need to be designed with high demands on range and precision. If the dynamic ranges of the A/D and D/A are increased, the resolution also needs to be increased in order to maintain the same quantization noise level. Therefore, an OFDM signal may require expensive A/Ds and D/As compared to many other modulation formats and for some applications suitable A/Ds and D/A may not be available at all. Also, a large power back-off (BO) of the amplifier is necessary. Intentional or accidental clipping of the OFDM signal often occurs in practice. The clipping of a received sample affects all subcarriers in the system. At least three concepts for reducing the PAPR have been proposed. In the first concept, one signal with a low PAPR out of a set of signals is transmitted. For instance, it is

observed that by appropriately choosing the phase of each subcarrier, the PAPR can be reduced.

The second concept reduces the PAPR by coding. It is shown that codes have good properties to combine both peak-to-average power reduction and forward error correction.

Finally, impulse-like time-domain functions are iteratively subtracted from the original signal to reduce the peaks. These time-domain signals are generated by a set of reserved, unused symbols in the DFT domain [11]. Subcarriers which are not used to transmit data symbols are used to transmit symbols, chosen to generate a transmitted signal with low PAPR.

Amplitude Clipping and Filtering

Among all these existing techniques, the iterative clipping and filtering (ICF) procedure may be the simplest to approach a specified PAPR threshold in the processed OFDM symbols [3, 4]. However, clipping time-domain signals causes out-of-band spectral regrowth and inband distortion. The latter can also degrade bit error performance of the OFDM system. In addition, frequency-domain filtering can reduce the spectral regrowth, but may still generate large time-domain peaks. For this reason, the ICF technique requires much iteration to approach a desired PAPR reduction.

The simplest technique for PAPR reduction might be amplitude clipping. Amplitude clipping limits the peak envelope of the input signal to a predetermined value or otherwise passes the input signal unperturbed. The distortion caused by amplitude clipping can be viewed as another source of noise. The noise caused by amplitude clipping falls both in band and out of band. In band distortion cannot be reduced by filtering and results in error performance degradation, while out of band radiation reduces spectral efficiency. Filtering after clipping can reduce out-of-band radiation but may also cause some peak regrowth so that the signal after clipping and filtering will exceed the clipping level at some points. To reduce overall peak regrowth, a repeated clipping and filtering operation can be used [11, 12].

Generally, repeated clipping and filtering takes good number of iterations to reach a desired amplitude level. In [13], a method to iteratively reconstruct the signal before clipping is proposed. This method is based on the fact that the effect of clipping noise is mitigated when decisions are made in the frequency domain. When the decisions are converted back to the time domain, the signal is recovered somewhat from the harmful effects of clipping, although this may not be perfect. To compensate for the performance degradation from clipping the clipped samples are

to be constructed based on the other samples in the over-sampled signals.

Channel Coding

Error control coding is an essential part of an OFDM system for mobile communication. OFDM in a fading environment is almost always used with coding to improve its performance. Coding such as turbo codes, low-density parity check codes and convolution codes can also be used to reduce the PAPR. A simple idea introduced in [13] is to select those codeword that minimize or reduce the PAPR for transmission. A more sophisticated approach proposed in [14] is to use codeword drawn from offsets from a linear code. The idea is to choose the code for its error correcting properties and the offset to reduce the PAPR of the resulting coded signals. This approach enjoys the twin benefits of PAPR reduction and error correction and is simple to implement but it requires extensive calculation to find good codes and offsets. A computationally efficient geometrical approach to offset selection is introduced in [15], but there is no guarantee about the amount of PAPR reduction that can be obtained with this approach.

Partial Transmit Sequence (PTS)

In the PTS technique, an input data block of N symbols is partitioned into disjoint sub blocks. The subcarriers in each sub block are weighted by a phase factor for that subblock [15–17]. The phase factors are selected such that the PAPR of the combined signal is minimized. In general, the selection of the phase factors is limited to a set with a finite number of elements to reduce the search complexity. So, it is necessary to perform an exhaustive search for $(M-1)$ phase factors. The search complexity increases exponentially with the number of sub blocks M . PTS needs M IDFT operations for each data block. The amount of PAPR reduction depends on the number of subblocks M and the number of allowed phase factors W [18, 19]. There are three kinds of subblock partitioning schemes: adjacent, interleaved and pseudo-random partitioning [20]. Among them, pseudo-random partitioning has been found to be the best choice. The PTS technique works with an arbitrary number of subcarriers and can have any modulation scheme.

The partial transmit sequence (PTS) [14] is a distortionless technique based on combining signal subblocks which are phase-shifted by constant phase factors. The technique can get sufficient PAPR reduction and side information need to be sent at the same time. But the exhaustive search complexity of the optimal phase combination increases exponentially with the number of sub-blocks. So many suboptimal PTS methods have been developed. The iterative flipping algorithm for PTS in [15]

has the computational complexity linearly proportional to the number of subblocks. A neighborhood search is proposed in [16] using gradient descent search. A suboptimal method in [17] is developed by modifying the problem into an equivalent problem of minimizing the sum of phase-rotated vectors. A simulated annealing method is proposed in [19]. A suboptimal PTS algorithm based on particle swarm optimization is proposed in [20, 21]. An intelligent genetic algorithm for PAPR reduction is developed [22, 23].

Considering that the usefulness of these techniques is limited to multicarrier systems with a small number of subcarriers and the required exhaustive search for a good code is intractable, the actual benefits of coding for PAPR reduction for practical multicarrier systems are limited.

However, for the traditional PTS (T-PTS) method, the communication system has to reserve some bits for the transmission of the phase rotation factors as side information (SI), resulting in a decrease in the data rate. It is to be noted that SI only represents the information about the phase rotation factors in this letter. Commonly, it is hard to correctly recover the SI at the receiver, which may largely increase the bit error rate (BER). When extra bits are employed to protect the SI for being correctly submitted, the total data rate is further degraded. In this letter, a novel method is proposed, which combines the channel estimation and T-PTS method to reduce the PAPR of OFDM signals, called as the Cross Entropy PTS method. Particularly, a virtual channel frequency response is considered as the combination of the traditional channel frequency response and the phase rotation factors of the T-PTS method [24–30]. Thus, the original OFDM signals could be directly recovered via channel estimation without any knowledge of the SI at the receiver. Therefore, the system does not need to reserve extra bits to deposit and protect the phase rotation factors. Furthermore, a novel pilot arrangement is also proposed, in which the pilot tones are independently inserted into each subblock to achieve an accurate channel estimation.

The Selected Mapping Technique (SLM)

In the SLM technique, the transmitter generates a set of sufficiently different candidate data blocks, all representing the same information as the original data block and selects the most favourable for transmission [21, 22]. Each data block is multiplied by U different phase sequences, each of length N , which resulting in modified data blocks. To include the unmodified data block in the set of modified data blocks, it is necessary to add the all-one vector of length N . Among the modified data blocks, the one with the lowest PAPR is selected for transmission. Information about the selected phase sequence should be transmitted to

the receiver as side information. At the receiver, the reverse operation is performed to recover the original data block. For implementation, the SLM technique needs U IDFT operations. This approach is applicable with all types of modulation and any number of subcarriers [22]. In [31–34] an SLM technique without explicit side information is proposed. To reduce the computational complexity while still improving the PAPR statistics, the quantum-inspired evolutionary algorithm (QEA), is introduced an effective algorithm that solves various combinatorial optimization problems, to determine a good set of subcarrier signs.

The Interleaving Technique

The interleaving technique for PAPR reduction is very similar to the SLM technique. In this approach, a set of interleaver is used to reduce the PAPR of the multicarrier signal instead of a set of phasesequences [23–25]. An interleaver is a device that operates on a block of N symbols and reorders or permutes them to make K modified data blocks, interleavers are used to produce permuted data blocks from the same data block. The PAPR of $(K - 1)$ permuted data blocks and that of the original data blocks are computed using K IDFT operations the data block with the lowest PAPR is then chosen for transmission [35–37]. To recover the original data block, the receiver needs only to know which interleaver is used at the transmitter thus, the number of required side information bits. Both the transmitter and receiver store the permutation indices $\{p(n)\}$ in memory. Thus, interleaving and deinterleaving can be done simply. The amount of PAPR reduction depends on the number of interleavers ($K - 1$) and the design of the interleavers.

The Tone Reservation Technique (TR)

Tone reservation (TR) is an efficient technique to reduce the PAPR of a multicarrier signal. The TR method can reduce the PAPR value in the OFDM signals by utilizing the reserved subcarriers which are not used for data transmission. In this technique, the baseband signal could be modified. This method is based on adding a data-block-dependent time domain signal to the original multicarrier signal to reduce its peaks. This time domain signal can be easily computed at the transmitter and stripped off at the receiver [26]. For the TR technique, the transmitter does not send data on a small subset of subcarriers that are optimized for PAPR reduction [22]. The aim is to find the time domain signal to be added to the original time domain signal x such that the PAPR is reduced. If the frequency domain added to a vector X , the new time domain signal can be represented as $x + c = \text{IDFT}\{X + C\}$, where c is the time domain signal due to C . The TR technique restricts

the data block X and peak reduction vector C to lie in disjoint frequency subspaces [38–40].

Assume that there are two mutually exclusive subsets of subcarriers: S is the set of subcarriers used for the data transmission and R is the set of remaining subcarriers used as the reserved tones. Basically, the value of C_n can be adjusted to reduce the peak value of x_k without disturbing the actual data contained in Xm . Thus, C_n must be investigated to minimize the maximum norm of the time domain signal x_k .

Since the subcarriers are orthogonal, these additional signals cause no distortion on the data bearing subcarriers. To find the value of C_n , convex optimization problem should be solved that can easily be cast as a linear programming (LP) problem. To reduce the computational complexity of LP, a simple gradient algorithm is also proposed in [22]. In the case of DMT for wire line systems, there are typically subcarriers with SNRs too low for sending any information, so these subcarriers must go unused and are available for PAPR reduction. In wireless systems however, there is typically no fast reliable channel state feedback to dictate whether some subcarriers should not be used [37–39]. Instead, a set of subcarriers must be reserved regardless of received SNRs, resulting in a bandwidth sacrifice.

In this technique, a portion of subcarriers (tone), not being used for data transmission, are reserved to create a dummy data in time domain which can minimize the PAPR of the overall signal. It is to be noted that since the dummy data on the reserved tone is separated (in frequency domain) from the data transmitting carriers, the data is not distorted and hence, the BER performance will not be degraded [7, 8]. Furthermore, TR does not require any side information to be sent to the receiver. Thus the dummy data can be easily discarded at the receiver after the FFT processing. Theoretically, the dummy data in TR technique can be found by minimizing of PAPR value via standard direct optimization technique which may cause high computationally complexity.

The Tone Injection Technique (TI)

Tone injection (TI) [8, 9] is a distortion less technique that can reduce PAPR significantly without data rate loss. In addition, TI does not require the exchange of side information between transmitter and receiver. However, implementation of the TI approach requires solving a difficult integer programming problem whose complexity grows exponentially with the number of available subcarriers, which is far too much to be practically implemented. Therefore, one has to resort to suboptimal solutions such as the greedy method.

The basic idea here is to increase the constellation size so that each of the points in the original basic constellation

can be mapped into several equivalent points in the expanded constellation [27]. Since each symbol in a data block can be mapped into one of several equivalent constellation points, these extra degrees of freedom can be exploited for PAPR reduction [28]. This method is called tone injection because substituting a point in the basic constellation for a new point in the larger constellation is equivalent to injecting a tone of the appropriate frequency and phase in the multicarrier signal. These methods expand the conventional QAM constellation by using redundant signaling representations for the same group of bits (a symbol). In these schemes, valid alternative representations of the original symbols on different subcarriers are generated first and then the corresponding PAPRs are calculated. The OFDM frame with the minimum PAPR is actually chosen for transmission into the channel.

It is to be assumed that M-ary square quadrature amplitude modulation (QAM) is used as a modulation scheme and the minimum distance between constellation points is d . Then the real part, imaginary part and the amount of PAPR reduction depends on number of modified symbols in a data block [40]. The TI technique may be more problematic than the TR technique since the injected signal occupies the same frequency band as the information bearing signal. The TI technique may also result in a power increase in the transmit signal due to the injected signal.

The Active Constellation Extension Technique (ACE)

Active constellation extension (ACE) is a PAPR reduction technique similar to TI [27]. In this technique, some of the outer signal constellation points in the data block are dynamically extended toward the outside of the original constellation such that the PAPR of the data block is reduced. The main idea of this scheme is easily explained in the case of a multicarrier signal with QPSK modulation in each subcarrier. In each subcarrier, there are four possible constellation points that lie in each quadrant in the complex plane and are equidistant from the real and imaginary axes [41–43]. Assuming white Gaussian noise, the maximum likelihood decision regions are the four quadrants bounded by the axes thus, a received data symbol is decided according to the quadrant in which the symbol is observed. Any point that is farther from the decision boundaries than the nominal constellation point (in the proper quadrant) will offer increased margin, which guarantees a lower BER [28–30]. Therefore modification can be allowed for constellation points within the quarter-plane outside of the nominal constellation point with no degradation in performance. If adjusted intelligently, a combination of these additional signals can be used to partially cancel time domain peaks in the transmit signal. The ACE idea can be applied together constellations as well, such as

QAM and MPSK constellations, because data points that lie on the outer boundaries of the constellations.

Criteria for Selection of PAPR Reduction Technique

There are many factors that should be considered before a specific PAPR reduction technique is chosen:

PAPR Reduction Capability

This is the most important factor in choosing a PAPR reduction technique. Careful attention must be paid to the fact that some techniques result in other harmful effects. For example, the amplitude clipping technique clearly removes the time domain signal peaks, but results in in-band distortion and out-of-band radiation [44–46].

Power Increase in Transmit Signal

Some techniques require a power increase in the transmit signal after using PAPR reduction techniques. For example, TR requires more signal power because some of its power must be used for the PRCs. TI uses a set of equivalent constellation points for an original constellation point to reduce PAPR. Since all the equivalent constellation points require more power than the original constellation point, the transmit signal will have more power after applying TI [47]. When the transmit signal power should be equal to or less than that before using a PAPR reduction technique, the transmit signal should be normalized back to the original power level, resulting in BER performance degradation for these techniques.

BER Increase at the Receiver

This is also an important factor and closely related to the power increase in the transmit signal. Some techniques may have an increase in BER at the receiver if the transmit signal power is fixed or equivalently may require larger transmit signal power to maintain the BER after applying the PAPR reduction technique. For example, the BER after applying ACE will be degraded if the transmit signal power is fixed. In some techniques such as SLM, PTS and interleaving, the entire data block may be lost if the side information is received in error. This may also increase the BER at the receiver [48, 49].

Loss in Data Rate

Some techniques require the data rate to be reduced. The block coding technique requires one out of four information symbols to be dedicated to control PAPR. In SLM, PTS and interleaving the data rate is reduced due to the

side information used to inform the receiver of what has been done in the transmitter [11–13]. In these techniques the side information may be received in error unless some form of protection such as channel coding is employed. When channel coding is used, the loss in data rate due to side information is increased further.

Computational Complexity

Computational complexity is another important consideration in choosing a PAPR reduction technique. Techniques such as PTS find a solution for the PAPR reduced signal by using much iteration. The PAPR reduction capability of the interleaving technique is better for a larger number of interleavers. Generally, more complex techniques have better PAPR reduction capability.

Other Considerations

Many of the PAPR reduction techniques do not consider the effect of the components in the transmitter such as the transmit filter, digital-to-analog (D/A) converter and transmit power amplifier. In practice, PAPR reduction techniques can be used only after careful performance and cost analyses for realistic environments. There are many factors to consider before a specific PAPR reduction technique is chosen. These factors include PAPR reduction capability, power increase in transmit signal, BER increase at the receiver, loss in data rate, computational complexity increase and so on.

Conclusion

Multicarrier transmission is a very attractive technique for high-speed transmission over a dispersive communication channel. The PAPR problem is one of the important issues to be addressed in developing multicarrier transmission systems. In this article, some PAPR reduction techniques are described for multicarrier transmission. Many promising techniques to reduce PAPR have been proposed, all of which have the potential to provide substantial reduction in PAPR at the cost of loss in data rate, transmit signal power increase, BER increase, computational complexity increase and so on. No specific PAPR reduction technique is the best solution for all multicarrier transmission systems. Rather, the PAPR reduction technique should be carefully chosen according to various system requirements. In practice, the effect of the transmit filter, D/A converter and transmit power amplifier must be taken into consideration to choose an appropriate PAPR reduction technique.

References

1. R.W. Chang, Synthesis of band-limited orthogonal signals for multichannel data transmission. *Bell Syst. Tech. J.* **46**(12), 1775–1796 (1966)
2. B.R. Saltzberg, Performance of an efficient parallel data transmission system. *IEEE Trans. Commun.* **15**(6), 805–811 (1967)
3. R.W. Chang, R.A. Gibby, A theoretical study of performance of an orthogonal multiplexing data transmission scheme. *IEEE Trans. Commun.* **16**(4), 529–540 (1968)
4. S.B. Weinstein, P.M. Ebert, Data transmission by frequency-division multiplexing using the discrete fourier transform. *IEEE Trans. Commun.* **19**(5), 628–634 (1971)
5. L.J. Cimini Jr, Analysis and simulation of a digital mobile channel using orthogonal frequency division multiplexing. *IEEE Trans. Commun.* **33**(7), 665–675 (1985)
6. J.A.C. Bingham, Multicarrier modulation for data transmission: an idea whose time has come. *IEEE Commun. Mag.* **28**(5), 5–14 (1990)
7. M. Alardand, R. Lasalle, Principles of modulation and channel coding for digital broadcasting for mobile receivers. *EBU Rev.* **224**, 47–69 (1987)
8. U. Reimers, Digital video broadcasting. *IEEE Commun. Mag.* **36**(10), 104–110 (1998)
9. B.R. Saltzberg, Comparison of single-carrier and multitone digital modulation for ADSL applications. *IEEE Commun. Mag.* **36**(11), 114–121 (1998)
10. R. O'Neill, L.B. Lopes, in *Envelope Variations and Spectral Splatter in Clipped Multicarrier Signals*. Proceedings IEEE PIMRC '95, Toronto, Canada, pp. 71–75, Sept 1995
11. X. Li, L.J. Cimini Jr, Effect of clipping and filtering on the performance of OFDM. *IEEE Commun. Lett.* **2**(5), 131–133 (1998)
12. J. Armstrong, Peak-to-average power reduction for OFDM by repeated clipping and frequency domain filtering. *Electron. Lett.* **38**(8), 246–247 (2002)
13. H. Chen, M. Haimovish, Iterative estimation and cancellation of clipping noise for OFDM signals. *IEEE Commun. Lett.* **7**(7), 305–307 (2003)
14. A.E. Jones, T.A. Wilkinson, Block coding scheme for reduction of peak to mean envelope power ratio of multicarrier transmission scheme. *Electron. Lett.* **30**(22), 2098–2099 (1994)
15. A.E. Jones, T.A. Wilkinson, in *Combined Coding for Error Control and Increased Robustness to System Nonlinearities in OFDM*. Proceedings IEEE VTC '96, Atlanta, GA, pp. 904–908, April–May 1996
16. V. Tarokh, H. Jafarkhani, On the computation and reduction of the peak-to-average power ratio in multicarrier communications. *IEEE Trans. Commun.* **48**(1), 37–44 (2000)
17. M. Golay, Complementary series. *IEEE Trans. Inf. Theory* **7**(2), 82–87 (1961)
18. J.A. Davis, J. Jedwab, Peak-to-mean power control and error correction for OFDM transmission using golay sequences and reed-muller codes. *Electron. Lett.* **33**(4), 267–268 (1997)
19. J.A. Davis, J. Jedwab, Peak-to-mean power control in OFDM, golay complementary sequences, and Reed–Muller codes. *IEEE Trans. Inf. Theory* **45**(7), 2397–2417 (1999)
20. K. Patterson, Generalized Reed–Muller codes and power control in OFDM modulation. *IEEE Trans. Inf. Theory* **46**(1), 104–120 (2000)
21. K.G. Paterson, V. Tarokh, On the existence and construction of good codes with low peak-to-average power ratios. *IEEE Trans. Inf. Theory* **46**(6), 1974–1987 (2000)

22. C.V. Chong, V. Tarokh, A simple encodable/decodable OFDM QPSK code with low peak-to-mean envelope power ratio. *IEEE Trans. Inf. Theory* **47**(7), 3025–3029 (2001)
23. B.S. Krongold, D.L. Jones, An active set approach for OFDM PAR reduction via tone reservation. *IEEE Trans. Signal Process.* **52**(2), 495–509 (2004)
24. L.J. Cimini (Jr.), B. Daneshrad, N.R. Sollenberger, in *Clustered OFDM with Transmitter Diversity and Coding*. Proceedings of the IEEE GLOBECOM'96, London, UK, pp. 703–707, Nov 1996
25. J. Tellado, in *Peak to Average Power Reduction for Multicarrier Modulation*. Ph.D. Dissertation, Stanford University, 2000
26. B.S. Krongold, D.L. Jones, PAR reduction in OFDM via active constellation extension. *IEEE Trans. Broadcast.* **49**(3), 258–268 (2003)
27. S.H. Müller, J.B. Huber, OFDM with reduced peak-to-average power ratio by optimum combination of partial transmit sequences. *Electron. Lett.* **33**(5), 368–369 (1997)
28. L.J. Cimini Jr, N.R. Sollenberger, Peak-to-average power ratio reduction of an OFDM signal using partial transmit sequences. *IEEE Commun. Lett.* **4**(3), 86–88 (2000)
29. C. Tellambura, Improved phase factor computation for the PARR of an OFDM signal using PTS. *IEEE Commun. Lett.* **5**(4), 135–137 (2001)
30. S.H. Han, J.H. Lee, PAPR reduction of OFDM signals using a reduced complexity PTS technique. *IEEE Signal Process. Lett.* **11**(11), 887–890 (2004)
31. S.H. Muller, J.B. Huber, in *A comparison of Peak Power Reduction Schemes for OFDM*. Proceedings of the IEEE GLOBECOM '97, Phoenix, AZ, pp. 1–5, Nov 1997
32. S.H. Müller, J.B. Huber, in *A Novel Peak Power Reduction Scheme for OFDM*. Proceedings of the IEEE PIMRC '97, Helsinki, Finland, pp. 1090–1094, Sept 1997
33. A.D.S. Jayalath, C. Tellambura, Adaptive PTS approach for reduction of peak-to-average power ratio of OFDM signal. *Electron. Lett.* **36**(14), 1226–1228 (2000)
34. N. Carson, T. A. Gulliver, Peak-to-average power ratio reduction of OFDM using repeat-accumulate codes and selective mapping. *Proceedings of the IEEE International Symposium on Information Theory*, p. 244, July 2002
35. R.W. Bäuml, R.F.H. Fisher, J.B. Huber, Reducing the peak-to-average power ratio of multicarrier modulation by selected mapping. *Electron. Lett.* **32**(22), 2056–2057 (1996)
36. H. Breiling, S.H. Müller-Weinfurtner, J.B. Huber, SLM peak-power reduction without explicit side information. *IEEE Commun. Lett.* **5**(6), 239–241 (2001)
37. G.R. Hill, M. Faulkner, J. Singh, Reducing the peak-to-average power ratio in OFDM by cyclically shifting partial transmit sequences. *Electron. Lett.* **36**(6), 560–561 (2000)
38. P. Van Eetvelt, G. Wade, M. Tomlinson, Peak to average power reduction for OFDM schemes by selective scrambling. *Electron. Lett.* **32**(21), 1963–1964 (1996)
39. A.D.S. Jayalath, C. Tellambura, Reducing the peak to-average power ratio of orthogonal frequency division multiplexing signal through bit or symbol interleaving. *Electron. Lett.* **36**(13), 1161–1163 (2000)
40. C. Tellambura, Computation of the continuous-time PAPR of an OFDM signal with BPSK subcarriers. *IEEE Commun. Lett.* **5**(5), 185–187 (2001)
41. R.V. Nee, R. Prasad, in *OFDM for Wireless Multimedia Communications*. (Artech House, USA, 2000)
42. H. Ochiai, H. Imai, On the distribution of the peak-to-average power ratio in OFDM signals. *IEEE Trans. Commun.* **49**(2), 282–289 (2001)
43. S. Wei, D.L. Goeckel, P.E. Kelly, in *A Modern Extreme Value Theory Approach to Calculating the Distribution of the paper in OFDM Systems*. Proceedings of the IEEE ICC2002, New York, NY, pp. 1686–1690, May 2002
44. M. Sharif, M. Gharavi-Alkhansari, B.H. Khalaj, On the peak-to-average power of OFDM signals based on oversampling. *IEEE Trans. Commun.* **51**(1), 72–78 (2003)
45. G. Wunder, H. Boche, Upper bounds on the statistical distribution of the crest-factor in OFDM transmission. *IEEE Trans. Inf. Theory* **49**(2), 488–494 (2003)
46. J. Heiskala, J. Terry, in *OFDM Wireless LANS: A Theoretical and Practical Guide*. (Sams Publishing, USA, 2002)
47. D. Kim, G.L. Stüber, Clipping noise mitigation for OFDM by decision-aided reconstruction. *IEEE Commun. Lett.* **3**(1), 4–6 (1999)
48. H. Saeedi, M. Sharif, F. Marvasti, Clipping noise cancellation in OFDM systems using oversampled signal reconstruction. *IEEE Commun. Lett.* **6**(2), 73–75 (2002)
49. R. Dinis, P. Montezuma, A. Gusmao, in *Performance Trade-offs with Quasi-Linearily Amplified OFDM Through a Two-Branch Combining Technique*. Proceedings of the IEEE VTC'96, Atlanta, GA, pp. 899–903, April–May 1996